



저작자표시-비영리-동일조건변경허락 2.0 대한민국

이용자는 아래의 조건을 따르는 경우에 한하여 자유롭게

- 이 저작물을 복제, 배포, 전송, 전시, 공연 및 방송할 수 있습니다.
- 이차적 저작물을 작성할 수 있습니다.

다음과 같은 조건을 따라야 합니다:



저작자표시. 귀하는 원저작자를 표시하여야 합니다.



비영리. 귀하는 이 저작물을 영리 목적으로 이용할 수 없습니다.



동일조건변경허락. 귀하가 이 저작물을 개작, 변형 또는 가공했을 경우에는, 이 저작물과 동일한 이용허락조건하에서만 배포할 수 있습니다.

- 귀하는, 이 저작물의 재이용이나 배포의 경우, 이 저작물에 적용된 이용허락조건을 명확하게 나타내어야 합니다.
- 저작권으로부터 별도의 허가를 받으면 이러한 조건들은 적용되지 않습니다.

저작권법에 따른 이용자의 권리는 위의 내용에 의하여 영향을 받지 않습니다.

이것은 [이용허락규약\(Legal Code\)](#)을 이해하기 쉽게 요약한 것입니다.

[Disclaimer](#)

Thesis for the Degree of Doctor of Philosophy

Nano- and Micro-Scaled Zinc Oxide and
Ni and Co Doped Zinc Oxide Materials:
Shape-Controlled Syntheses and
Characterizations

The logo of Pukyong National University is a circular emblem. It features a stylized blue and white design in the center, resembling a compass or a stylized 'P'. The words 'PUKYONG NATIONAL UNIVERSITY' are written in a circular path around the center. Below the English text, there is Korean text: '부산대학교' (Pusan National University).

by

Xiao Li Zhang

Department of Chemistry

The Graduate School

Pukyong National University

August 2008

Nano- and Micro-Scaled Zinc Oxide and Ni and Co Doped Zinc Oxide Materials: Shape-Controlled Syntheses and Characterizations

(Zinc Oxide 와 Ni, Co 가 도핑된 Zinc
Oxide 나노 및 마이크로 크기의
물질: 형상제어 합성 및 특성 연구)

Advisor: Professor Ju Chang Kim

by
Xiao Li Zhang

A thesis submitted in partial fulfillment of the requirements
for the degree of

Doctor of Philosophy

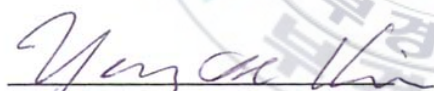
in the Department of Chemistry, The Graduate School,
Pukyong National University

August 2008

Nano- and Micro-Scaled Zinc Oxide and Ni and Co Doped Zinc
Oxide Materials: Shape-Controlled Syntheses and
Characterizations

A dissertation
by
Xiao Li Zhang

Approved by:


Chairman Yeong Il Kim


Member Ju Chang Kim


Member Young Soo Kang


Member Dong Jae Lee


Member Sung Doo Moon

August, 2008

Nano- and Micro-Scaled Zinc Oxide and Ni and Co Doped Zinc Oxide

Materials: Shape-Controlled Syntheses and Characterizations

Xiao Li Zhang

Research Advisor: Professor Ju Chang Kim
Department of Chemistry, Graduate School of Natural Science,
Pukyong National University

Abstract

In the present study, perpendicular side-faceted zinc oxide nanorod, one-dimensional zinc nickel oxide solid solution, nickel and cobalt doped zinc oxide hollow spheres were successfully fabricated through facile one-pot template-free solvothermal methods. A surfactant-directed solvothermal synthesis approach has been successfully demonstrated on fabricating large scale of ZnO hybrid materials with diverse morphologies in a simple ethanol solution.

1. A novel route to the rational fabrication of narrow one-dimensional ZnO nanocrystals with perpendicular side facets is demonstrated in alcoholic solutions. The synthesis involves no-template or no-substrate solution method, which still allows the oriented growth of ZnO nanostructures at large-scale, low-cost, and moderate temperatures. The management consists of monitoring of the nucleation, growth, and aging processes by means of chemical and solvent control of the interfacial free energy. It enables the control of the size of nano-, meso-, and microcrystallites with various aspects from cubes to rods, wires, and belts.

2. A novel facile method has been demonstrated for large-scale synthesis of zinc oxide based one-dimensional solid solution with a series percentage of nickel dopant.

The obtained $\text{Zn}_{1-x}\text{Ni}_x\text{O}$ nanorods were characterized by X-ray diffraction, transmission electron microscopy, selected area electron diffraction and energy dispersed X-ray spectroscopy. The result shows that the obtained $\text{Zn}_{1-x}\text{Ni}_x\text{O}$ nanorods are single crystalline with the Ni^{2+} dopants occupying tetrahedral Zn^{2+} cation sites of wurtzite ZnO . Moreover, the $\text{Zn}_{1-x}\text{Ni}_x\text{O}$ nanorods exhibit robust high-Curie-Temperature (T_C) ferromagnetism at 300 K.

3. This chapter describes a template-free solvothermal treatment of precursors in methanol solvent leading to the formation of transition-metal-doped zinc oxide spheres and hollow spheres is reported. The synthesis includes hydrolysis of metal salts, spontaneous aggregation and localized Ostwald ripening in an alcohol solvent. Electron microscopy observation and X-ray diffraction analysis confirmed that the mesoscale hollow spheres with uniform in size and shape and highly crystalline structures are finely doped with transition metals such as nickel or cobalt. Magnetic hysteresis loops reveal robust coercivities at 300 K, indicating high- T_C ferromagnetism in the system.

4. A novel surfactant-directed process is successfully developed for morphology control on ZnO hybrid materials with distinctive shapes ranging from mushroom, bi-hemispheres, dumbbell, bi-layer hexagonal disks, to flower-like aggregated sheets. Replacing of the conventional oil-water system, a simple alcohol-water surfactant system is employed that provides a more environmental benign and bio-safe approach. Moreover, the remarkable ZnO hybrid materials and facile method demonstrated here not only expand the material morphologies but also provide a new approach to explore the materials for physical and chemical properties and technological applications.

Contents

Abstract	i
Chapter 1. Introduction	1
1. Introduction of Material Science and Engineering	1
2. Introduction of Nanomaterials	1
3. Size and Shape Dependence of Properties	2
4. Introduction of Semiconductor	5
5. Introduction of Zinc Oxide	6
6. Synthetic Methods of Nanomaterials	8
7. Shape-Controlled Synthesis of Zinc Oxide Materials	11
8. Objectives of Research	12
9. Reference	15
Chapter 2. Large-scale Synthesis of Perpendicular Side-Faceted One-Dimensional ZnO Nanocrystals	18
1. Introduction	18
2. Experiment	19
3. Result and discussion	20
4. Conclusion	28
5. Reference	28
Chapter 3. Large-scale synthesis of one-dimensional zinc nickel oxide solid solution	31
1. Introduction	31
2. Experiment	32
3. Result and discussion	33
4. Conclusion	39
5. Reference	39
Chapter 4. Inorganic cluster synthesis and characterization of transition metal-doped ZnO hollow spheres	42

1. Introduction	42
2. Experiment	43
3. Result and discussion	44
4. Conclusion	53
5. Reference	54
Chapter 5. Surfactant-directed fabrication of ZnO with tunable morphology	58
1. Introduction	58
2. Experiment	59
3. Result and discussion	60
4. Conclusion	69
5. Reference	70
Summary (in korean)	73
Acknowledgement	74
Publications	75



Chapter 1. Introduction

1.1. Introduction of Material Science and Engineering

In recent years, MSE has attracted particular attention because of the dramatic discovery of unusual materials, the ingenious development of novel processing methods, and the significant improvement of mechanical, chemical, electrical, optical, and magnetic properties. The essential framework of MSE is composed of the scientific and practical interrelationships at play among the processing, structure, properties, and performance of all classes of materials that are potentially useful to society. This linkage is illustrated in Figure 1-1. Overall, MSE operates to (a) generate new knowledge toward a deeper understanding of materials as a substantive component of nature, and then to (b) harness this knowledge effectively in the service of mankind.¹

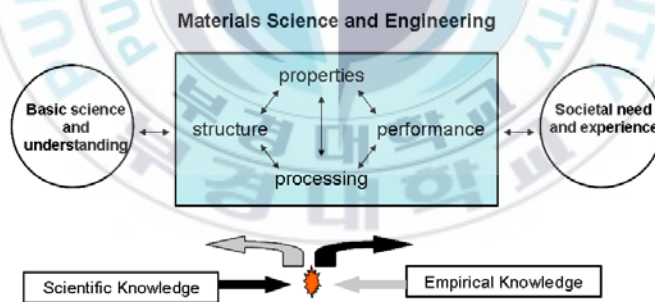


Figure 1-1. A model of materials science and engineering as an interactive information-transfer network, linking the interrelationships among the structure, properties, processing, and performance of materials, and highlighting the countercurrent flows of scientific and empirical knowledge.

1.2. Introduction of Nanomaterials

Technology in the twenty first century requires the miniaturization of devices into nanometer sizes while their ultimate performance is dramatically enhanced. This raises many issues regarding to new materials for achieving specific functionality

and selectivity. Nanomaterials, a new branch of MSE, are attracting a great deal of attention because of their potential applications in areas such as electronics, optics, catalysis, ceramics, magnetic data storage, and nanocomposites. The unique properties and the improved performances of nanomaterials are determined by their sizes, surface structures and interparticle interactions. Nanotechnology is based on the recognition that particles less than the size of 100 nm impart to nanostructures built from them new properties and behavior. This happens because particles which are smaller than the characteristic lengths associated with particular phenomena often display new chemistry and physics, leading to new behavior which depends on the size. The dependence of the behavior on the particle size can allow one to engineer their properties. The role played by particles size is comparable, in some cases, to the particle chemical composition, adding another flexible parameter for designing and controlling their behavior.^{2,3} Nanomaterials contain nanostructured materials and nanophase/nanoparticle materials. Nanostructured materials refer to condensed bulk materials that are made of grains with grain sizes in the nanometer scale, while another are usually the dispersive nanoparticles.

1.3. Size and Shape Dependence of Properties

Many properties of solids depend on the size range over which they are measured. Microscopic details become average when investigating bulk materials. When the measurements are made in the micrometer or nanometer range, many properties of materials change, such as mechanical, ferroelectric, and ferromagnetic properties. Nanomaterials are a bridge that links single elements with single crystalline bulk structures. Quantum mechanics has successfully described the electronic structures of single elements and single crystalline bulks. The well established bondings, such as ionic, covalent, metallic and secondary, are the basis of solid state structure. The

theory for transition in energy levels from discrete for fundamental elements to continuous bands for bulk is the basis of many electronic properties. Therefore a thorough understanding on the structure of nanocrystals can provide deep insight in the structural evolution from single atoms to crystalline solids.

3-1. Quantum effect

A high percentage of surface atoms introduces many size-dependent phenomena. The finite size of the particle confines the spatial distribution of the electrons, leading to the quantized energy levels due to size effect. This quantum confinement has applications in semiconductors, optoelectronics and non-linear optics. The spherical-like shape of nanocrystals produces surface stress (positive or negative), resulting in lattice relaxation (expansion or contraction) and change in lattice constant.⁴ It is known that the electron energy band structure and bandgap are sensitive to lattice constant. The lattice relaxation introduced by nanocrystal size could affect its electronic properties.

3-2 Catalytic properties

A large percentage of surface atoms greatly increase surface activities, thus the most important application of nanocrystals has been in catalysis. The unique surface structure, electronic states and largely exposed surface area are required for stimulating and promoting chemical reactions. The size-dependent catalytic properties of nanocrystals have been widely studied, while investigations on the shape (facet)-dependent catalytic behavior are cumbersome.⁵

3-3. Mechanical properties

It is known that mechanical properties of a solid depend strongly on the density of dislocations, interface-to-volume ratio and grain size. An enhancement in damping capacity of a nanostructured solid may be associated with grain-boundary sliding or

with energy dissipation mechanism localized at interfaces.⁶ A decrease in grain size significantly affects the yield strength and hardness.⁷ The grain boundary structure, boundary angle, boundary sliding and movement of dislocations are important factors that determine the mechanical properties of the nanostructured materials.

3-4. Magnetic properties

The magnetic properties of nano-size particles differ from those of bulk mainly in two points. The large surface-to-volume ratio results in a different local environment for the surface atoms in their magnetic coupling/interaction with neighboring atoms, leading to the mixed volume and surface magnetic characteristics. Unlike bulk ferromagnetic materials, which usually form multiple magnetic domains, several small ferromagnetic particles could consist of only a single magnetic domain. In the case of a single particle being a single domain, the superparamagnetism occurs, in which the magnetizations of the particles are randomly distributed and they are aligned only under an applied magnetic field, and the alignment disappears once the external field is withdrawn. In ultra-compact information storage, for example, the size of the domain determines the limit of storage density.⁸ Magnetic nanocrystals have other important applications such as in color imaging, bioprocessing, magnetic refrigeration, and ferrofluids.⁹ Moreover, metallic heterostructured multilayers comprised of alternating ferromagnetic and nonmagnetic layers have been found to exhibit giant magnetoresistance (GMR), a significant change in the electrical resistance experienced by current flowing parallel to the layers when an external magnetic field is applied.¹⁰ GMR has important applications in data storage and sensors.

3-5. Thermodynamic properties

The large surface-to-volume ratio of nanocrystals greatly changes the role played

by surface atoms in determining their thermodynamic properties. The reduced coordination number of the surface atoms greatly increases the surface energy so that atom diffusion occurs at relatively lower temperatures.¹¹ Nanocrystals usually have faceted shape and mainly enclosed by low index crystallographic planes. It is possible to control the particle shape, for example, cubic Pt nanocrystals bounded by {100} facets and tetrahedral Pt nanocrystals enclosed by {111} facets.^{5(a)} The rod-like Au nanocrystals have also been synthesized, which are enclosed by {100} and {110} facets.^{5(b)} The density of surface atoms changes significantly for different crystallographic planes, possibly leading to different thermodynamic properties.

1.4. Introduction of Semiconductor

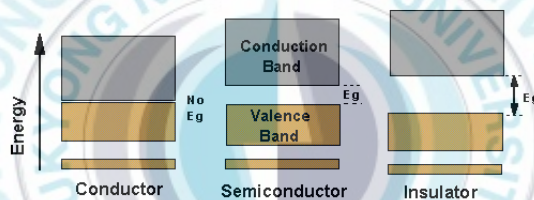


Figure 1-2. Energy bands of a conductor, an intrinsic semiconductor and an insulator.

When a solid is formed the energy levels of the atoms broaden and form bands with forbidden gaps between them. The electrons can have energy values that exist within one of the bands, but cannot have energies corresponding to values in the gaps between the bands. In semiconductors the gap energy (E_g) is small, but large enough so that a fairly small number of electrons are in the conduction band due to thermal energy ($k_B T$). The density of electrons reaching the conduction band by this thermal excitation process is relatively low, but by no means negligible, so the electrical conductivity is small; hence the term semiconducting. A material of this type is called an intrinsic semiconductor.

Impurities alter the semiconducting characteristics of materials by introducing

excess electrons or excess electron holes. A semiconductor can be doped with donor atoms that give electrons to the conduction band where they can carry current, so called n-type semiconductor. The material can also be doped with acceptor atoms that obtain electrons from the valence band and leave behind positive charges called holes that can also carry current. This type material is called p-type semiconductor. These two types of conductivity in semiconductors are temperature- dependent, as is the intrinsic semiconductivity.^{1,3}

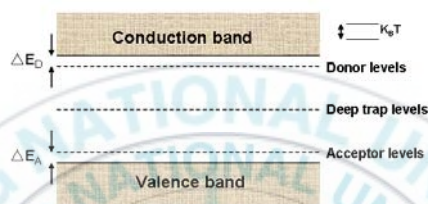


Figure 1-3. Sketch of the forbidden energy gap showing acceptor levels the typical distance Δ_A and donor levels the typical distance Δ_D . The value of the thermal energy $k_B T$ is indicated on the right.

1.5.Introduction of Zinc Oxide

5-1. Physical properties

Zinc oxide is a unique material that exhibits semiconducting and piezoelectric dual properties. ZnO is a key technological material. The lack of a centre of symmetry in wurtzite, combined with large electromechanical coupling, results in strong piezoelectric and pyroelectric properties and the consequent use of ZnO in mechanical actuators and piezoelectric sensors. In addition, ZnO is a wide band-gap (3.37 eV) compound semiconductor that is suitable for short wavelength optoelectronic applications. The high exciton binding energy (60 meV) in ZnO crystal can ensure efficient excitonic emission at room temperature and room temperature ultraviolet (UV) luminescence has been reported in disordered nanoparticles and thin films. ZnO is transparent to visible light and can be made

highly conductive by doping.¹²

5-2. Crystal structure

Wurtzite zinc oxide has a hexagonal structure (space group $C6_{mc}$) with lattice parameters $a = 0.3296$ and $c = 0.52065$ nm. The structure of zinc oxide can be simply described as a number of alternating planes composed of tetrahedrally coordinated O^{2-} and Zn^{2+} ions, stacked alternately along the c -axis (Figure 1-4). The tetrahedral coordination in ZnO results in noncentral symmetric structure and consequently piezoelectricity and pyroelectricity. Another important characteristic of ZnO is polar surfaces. The most common polar surface is the basal plane. The oppositely charged ions produce positively charged Zn-(0001) and negatively charged O-(0001) surfaces, resulting in a normal dipole moment and spontaneous polarization along the c -axis as well as a divergence in surface energy. To maintain a stable structure, the polar surfaces generally have facets or exhibit massive surface reconstructions, but $ZnO-\pm(0001)$ are exceptions: they are atomically flat, stable and without reconstruction.¹³ Efforts to understand the superior stability of the $ZnO \pm(0001)$ polar surfaces are at the forefront of research in today's surface physics.¹⁴ The other two most commonly observed facets for ZnO are $\{2-1-10\}$ and $\{0-1-10\}$, which are non-polar surfaces and have lower energy than the $\{0001\}$ facets.

5-3. Typical growth structures

Structurally, zinc oxide has three types of fast growth directions: $\langle 2-1-10 \rangle$, $\langle 01-10 \rangle$ and $\pm[0001]$. Together with the polar surfaces due to atomic terminations, ZnO exhibits a wide range of novel structures that can be grown by tuning the growth rates along these directions. One of the most profound factors determining the morphology involves the relative surface activities of various growth facets under given conditions. Macroscopically, a crystal has different kinetic parameters

for different crystal planes, which are emphasized under controlled growth conditions. Thus, after an initial period of nucleation and incubation, a crystallite will commonly develop into a three-dimensional object with well-defined, low index crystallographic faces.

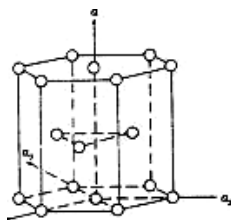


Figure 1-4. Crystal structure of zinc oxide.

1.6. Synthesis Methods of Nanomaterials

6-1. Solution phase methods

6-1-1. Sol-gel method

Sol-gel processing is a wet chemical synthesis approach that can be used to generate nanoparticles by gelation, precipitation, and hydrothermal treatment. The advantage of the sol-gel method of synthesis is that virtually any metal oxide system can be examined, and no special apparatus or equipment is required. In addition, the formation of ceramics of high purity and good control over microstructure and particle morphology in the synthesis, typically at room temperature. The precipitation of colloids has been reported that it may be accomplished in a wide variety of morphologies and grain sizes; however, in order to obtain different morphologies and size, extensive chemical modifications must be made for each metal oxide system studied.¹⁵

6-1-2. Micelle-template synthesis

The basis of micelle template synthetic methods is using a surfactant to stabilize varying aqueous droplet sizes in hydrocarbon medium. Metal salt precursors are

contained in the aqueous portion and are transformed by a reactant from the hydrocarbon phase. Both the structure of the surfactant and the steric size are able to produce metals having a wide range of grain size. Although notable grain-size control has been observed, the technique has a major disadvantage in that the commercial application may be limited due to the large amount of organic surfactant surrounding the crystals, and when this is removed by washing, the nanostructured grains normally grow.

6-1-3. Polymer-assisted synthesis

A new synthetic technique based on mediation of polymeric materials overcomes the problems associated with the large amounts of surfactants required in micelle processes. Some polymers are monodisperse, hyperbranched having a very high concentration of surface functional groups. The interesting aspect about the polymer-assisted methods is that the obtained nanostructures could be extracted into hydrocarbon solution, leaving the polymer behind.

6-1-4. Protein-mediated synthesis

Nanostructured materials were synthesized through developed new processes on hollow or highly oriented protein templates.¹⁶ The obtained nanomaterials can have varying grain size. However, the proteins are not stable at high temperatures that make this synthetic method with reaction temperature limitation.

6-1-5. Sonochemical Synthesis

The sonochemical process has been proved to be a useful technique for generating nanodimensional materials.¹⁷ Ultrasound irradiation offers a very attractive method for the preparation of novel materials with unusual properties and has shown very rapid growth in its application to materials science due to its unique reaction effects and ability to induce the formation of particles with much smaller sizes. An acoustic

cavitation process can generate a transient localized hot zone with extremely high temperature gradient and pressure. Such sudden changes in temperature and pressure assist the destruction of the sonochemical precursor (e.g., organometallic solution) and the formation of nanoparticles.

6-2. Vapor phase methods

Initial development of new crystalline materials was based on nanoparticles generated by evaporation and condensation (nucleation and growth) in a subatmospheric inert-gas environment. Various aerosol processing techniques have been reported to improve the production yield of nanoparticles. These include synthesis by combustion flame; plasma; laser ablation; chemical vapor condensation; spray pyrolysis; electrospray; and plasma spray.¹⁸

6-3. Other Strategies

Additional nanoparticle synthesis techniques include microemulsion processing, and high-energy ball milling.

In hydrodynamic cavitation, nanoparticles are generated through creation and release of gas bubbles inside the sol-gel solution. By rapidly pressurizing in a supercritical drying chamber and exposing to cavitation disturbance and high temperature heating, the sol-gel solution is mixed. The erupted hydrodynamic bubbles are responsible for nucleation, growth, and quenching of the nanoparticles. Particle size can be controlled by adjusting the pressure and the solution retention time in the cavitation chamber.

Microemulsions have been used for synthesis of metallic, semiconductor, silica, barium sulfate, magnetic, and superconductor nanoparticles. By controlling the very low interfacial tension ($\sim 10\text{--}3\text{ mN/m}$) through the addition of a cosurfactant (e.g., an alcohol of intermediate chain length), these microemulsions are produced

spontaneously without the need for significant mechanical agitation. The technique is useful for large-scale production of nanoparticles using relatively simple and inexpensive hardware.

Finally, high energy ball milling, the only top-down approach for nanoparticle synthesis, has been used for the generation of magnetic, catalytic, and structural nanoparticles. The technique, which is already a commercial technology, has been considered dirty because of contamination problems from ball-milling processes. However, the availability of tungsten carbide components and the use of inert atmosphere and/or high vacuum processes have reduced impurities to acceptable levels for many industrial applications. Common drawbacks include the low surface area, the highly polydisperse size distributions, and the partially amorphous state of the as-prepared powders.

1.7. Shape-Controlled Synthesis of Zinc Oxide Materials

Among the developed synthetic methods, vapor phase approaches have been used for fabricating a diversity of nano- or micro-scaled nanostructures, such as rods, wires, nails, belts, branches, combs, rings, cages and shells, at high temperature with its simplicity of process and high-quality of products.¹⁹ However, SVP approaches have major limitation in low yield. Solution phase synthetic approaches by thermal treatment of the reactant in different solvents media, may be the most simple and effective way to prepare sufficiently crystallized materials at relatively low temperatures, while exempted from further calcinations. Besides this, the benefits of a utilizing solution-based method have also involved the considerable influence of reaction species on the final size and morphology of the as-synthesized samples on a large scale.²⁰ Recent reports demonstrated that large polar surface of ZnO can be generated when the surface charge is compensated by using polymers and

surfactants as passivation agents.²¹ Micelles formed by surfactants can have various shapes from spheres, rods, ellipsoids, to disks, and even much more complex structures by adjusting experimental parameters. Therefore, size- and shape controlled nano- or microstructures can be fabricated through solution phase synthesis.²²

1.8. Objectives of Research

8-1. Large-scale synthesis of perpendicular side-faceted one-dimensional ZnO nanocrystals

Among the 1D semiconducting nanomaterials, as a versatile functional material, ZnO has a diverse group of growth morphologies, such as nanowires, nanorods, nanocombs, nanobelts, etc. Those kinds of nanostructures could have novel applications in optoelectronics, sensors, transducers, and biomedical science because ZnO is bio-safe. Although evaporation processes for various 1D ZnO nanostructures are favored for their simplicity and high-quality products described in the literatures, these gas-phase approaches generally require economically prohibitive temperatures of 800 – 1400 °C. In addition to the vapor phase deposition methods, the solution approaches to 1D ZnO nanostructures are appealing because of their low growth temperatures and good potential for scale-up. However, to the best of our knowledge, the wet chemical method usually need organic compound, such as diethylenetriamine, methenamine, or carbamide, as the templates. As an improvement, herein, our strategy to design one-dimensional ZnO nanostructures with perpendicular side-facets and varies aspects from cubes to rods, narrow wires (with diameter range down to 15 nm) and meso-, microcrystallites is based entirely on a wet chemical, bottom-up approach that synthesized, without template, from the theoretical modeling and experimental monitoring of the alcohol-oxide interfacial

thermodynamics and kinetics of nucleation, growth, and aging processes. Furthermore, this technique has already been successfully demonstrated by the fabrication of large, one-dimensional growth of other kinds of one-dimensional nanomaterials in our further work.

8-2. Large-scale synthesis of one-dimensional zinc nickel oxide solid solution

Led by the discovery of ferromagnetism in transition metal doped semiconductor, spintronics (spin-based electronics) has been deeply studied on both theories and experiments due to its enabling spin as well as the charge freedom of the carriers for new concept devices. Practically, this system has been experimentally studied, however, room temperature ferromagnetism has been reported in the vast majority of bulk materials, or thin films, or colloid, etc. ZnO based one-dimensional dilute magnetic solid solutions are of vital importance, since they not only play an important role as the building blocks of electronic and spintronic devices in the bottom-up milestone, but also provide excellent opportunities to study the effect of dimensionality and size on magnetism. To date, little work has been done on the fabrication of one-dimensional nanostructured $\text{Zn}_{1-x}\text{M}_x\text{O}$ through chemical vapor deposition (CVD) method, which has played as a superior since its quite effectiveness in producing a great amount of one-dimensional nanoscaled semiconductors. Nevertheless, the CVD methods are evidently limited in homogeneous doping at the extreme vapor-phased experimental condition. Herein, following our early work on non-surfactant synthesizing one-dimensional ZnO nanomaterials, we present a simple and facile method of large-scale synthesis of zinc oxide based one-dimensional solid solution with a series percentage of nickel dopant. Moreover, the synthetic process here also allows for the introduction of other transition metals, such as Co and Mn, etc.

8-3. Inorganic cluster synthesis and characterization of transition metal-doped ZnO hollow spheres

Spherical colloidal materials made of metals or semiconductors, especially with porous structure and hollow interior, have been the topic of extensive research. Such materials exhibit highly desirable optical, electronic, magnetic, and catalytic properties that can be designed during the fabrication process. The applications range from robust catalysts, drug delivery, photonic devices, artificial cells, and active-material encapsulation to ionic intercalation and size-selective reactors. In case of template-directed synthetic methods, to generate the hollow interiors, further treatments such as calcinations or dissolution were needed to remove the templates. Studies on zinc oxide based dilute magnetic semiconductors have involved synthesizing bulk materials, thin films, colloids and nanocrystals, and one-dimensional structures. Spherical structures such as mesoscale spheres and hollow spheres have not yet been reported. In this chapter, we demonstrate a template-free process for fabricating transition-metal-doped zinc oxide mesoscale spheres and hollow spheres with porous shells via initial aggregation followed by Ostwald ripening under solvothermal conditions.

8-4. Surfactant-directed fabrication of ZnO with tunable morphology

The optical, electronic and catalytic responses of a material depend on its particular size, shape, component, and local dielectric environment. In modern materials science, fabrication of size- and shape-controlled materials is one of the most important techniques in controlling their chemical and physical properties. Recent reports demonstrated that large polar surface of ZnO can be generated when the surface charge is compensated by using polymers and surfactants as passivation agents. Micelles formed by surfactants can have various shapes from spheres, rods,

ellipsoids, to disks, and even much more complex structures by adjusting experimental parameters. Therefore, size- and shape controlled nano- or microstructures can be fabricated through solution phase synthesis. Here we demonstrate a facile rational surfactant-directed morphology control on hybrid ZnO materials in an environmental benign alcohol-water reaction medium. ZnO hybrid materials with diverse shapes ranging from mushroom-like, double hemi-spheres, dumbbell, to hexagonal bi-layer disks and flower-like aggregation of sheets, can be easily prepared on a large scale.

References

1. Vlack, L. H. V., *Elements of Materials Science and Engineering*, Sixth Edition, Addison-Wesley Publishing Co., **1989**.
2. Wang, Z. L., *Characterization of Nanophase Materials*, First Edition, John Wiley & Sons Ltd, **2000**.
3. Poole, C. P. and Owens, F. J., *Introduction to Nanotechnology*, John Wiley & Sons Ltd, **2003**.
4. Woltersdorf, J.; Nepijko, A. S.; Pippel, E. *Surf. Sci.* **1981**, 106, 64.
5. (a) Ahmadi, T. S.; Wang, Z. L.; Green, T. C.; Henglein, A.; EL-Sayed, M A. *Science*, **1996**, 272, 1924. (b) Tian, N.; Zhou, Z.-Y.; Sun, S.-G.; Ding, Y.; Wang, Z. L. *Science*, **2007**, 316, 732; (c) Feldheim, D. L. *Science*, **2007**, 316, 699.
6. (a) Berry, B. S.; Pritchett, W. C. *Thin Solid Films*, **1976**, 33, 19; (b) Su, C. M.; Oberle, R. R.; Wutting, M.; Cammarata, R.C. *Mater. Res. Soc. Symp. Proc.*, **1993**, 280, 527.
7. Weertman, J. R.; Averback, R. S., *Nanomaterials: Synthesis, Properties and Applications*, eds. A. S. Edelstein and R. C. Cammarata, London, Institute of

- Phys. Publ., **1996**.
8. (a) Gunther, L. *Phys. World*, **1990**, 3, 28; (b) Audran, R. G.; Huguenard, A. P. *U.S. Patent*, **1981**, 4,302,523.
 9. Ziolo, R. F. *U.S. Patent*, **1984**, 4,474,866; (b) Marchessault, R. H.; Ricard, S.; Rioux, P. *Carbohydrate Res.*, **1992**, 224, 133; (c) McMichael, R. D.; Shull, R. D.; Swartzendruber, L. J.; Bennett, L. H.; Watson, R. E. *J. Magn. Magnsm Mater.*, **1992**, 111, 29; (d) Anton, I. et al. *J. Magn. Magnsm Mater.*, **1990**, 85, 219.
 10. Baibich, M. N.; Broto, J. M.; Fert, A.; Nguyen Van dau, F.; Petroff, F.; Etienne, P.; Greuzet, G.; Friederich, A.; Chazelas, J. *Phys. Rev. Letts.* **1988**, 61, 2472.
 11. Buffat, Ph.; Borel, J. P. *Phys. Rev. A* **1976**, 13, 2287.
 12. Wang, Z. L. *J. Phys.: Condens. Matter* **2004**, 16, R829.
 13. (a) Dulub, O.; Boatner, L. A.; Diebold, U. *Surf. Sci.* **2002**, 519, 201; (b) Meyer, B.; Marx, D. *Phys. Rev. B* **2003**, 67, 035403.
 14. (a) Tasker, P. W. *J. Phys. C: Solid State Phys.* **1979**, 12, 4977; (b) Dulub, O.; Diebold, U.; Kresse, G. *Phys. Rev. Lett.* **2003**, 90, 016102; (c) Wander, A.; Schedin, F.; Steadman, P.; Norris, A.; McGrath, R.; Turner, T. S.; Thornton, G.; Harrison, N. M. *Phys. Rev. Lett.* **2001**, 86, 3811; (d) Staemmler, V.; Fink, K.; Meyer, B.; Marx, D.; Kunat, M.; Gil Girol, S.; Burghaus, U.; Woll, Ch. *Phys. Rev. Lett.* **2003**, 90, 106102.
 15. Matijevic, E. Control of powder morphology, in *Chemical Processing of Advanced Materials* (Hench, L. H.; West, J. K.; Eds.), Wiley, New York **1992**.
 16. (a) Behrens, S.; Dinjus, E.; Unger, E. *Nachrichten* **1999**, 31, 117; (b) Behrens, S.; Habicht, W.; Boukis, N.; Dinjus, E.; Baum, M.; Unger, E. *Private communication from Behren, S.*, Institut für Technische Chemie,

Forschungszentrum Karlsruhe, Germany (2000).

17. (1) Dhas, N. A.; Zaban, A. and Gedanken, A. *Chem. Mater.* **1999**, *11*, 806; (2) Suslick, K. S. *Ultrasound: Its Chemical, Physical and Biological Effects*, VCH, Weinheim, Germany, **1998**; (3) Suslick, K. S.; Price, G. J. *Annu. Rev. Mater. Sci.* **1999**, *29*, 295; (4) Gates, B.; Mayers, B.; Grossman A. and Xia, Y. *Adv. Mater.* **2002**, *14*, 1749; (5). Prozorov, T.; Prozorov R. and Suslick, K. S. *J. Am. Chem. Soc.* **2004**, *126*, 13890.
18. (a) Karch, J.; Birringer R. and Gleiter, H. *Nature* **1987**, *330*, 556; (b) Uyeda, R. *Progress in Materials Science* **1991**, *35*, 1.
19. (a) Gao, P. X.; Wang, Z. L. *J. Am. Chem. Soc.* **2003**, *125*, 11299; (b) Hu J. Q.; Bando, Y.; Zhan, J. H.; Li, Y. B.; Sekiguchi, T. *Appl. Phys. Lett.* **2003**, *83*, 4414; (c) Park, W. I.; Yi, G.-C.; Kim, M.; Pennycook, S. J. *Adv. Mater.* **2002**, *14*, 1841; (d) Wu, J.-J.; Liu, S.-C. *Adv. Mater.* **2002**, *14*, 215; (e) Gao, P. X. and Wang, Z. L. *Nano Lett.* **2003**, *3*, 1315.
20. (a) Taubert, A.; Palms, D.; Weiss, Ö.; Piccini, M.-T.; Batchelder, D. N. *Chem. Mater.* **2002**, *14*, 2594; (b) Zhang, J.; Sun, L.; Yin, J.; Su, H.; Liao, C.; Yan, C. *Chem. Mater.* **2002**, *14*, 4172; (c) Yao, K. X.; Zeng, H. C. *J. Phys. Chem. B* **2006**, *110*, 14736;
21. (a) Li, F.; Ding, Y.; Gao, P.; Xin, X.; Wang, Z. L. *Angew. Chem. Int. Ed.* **2004**, *43*, 5238; (b) Peng, Y.; Xu. A.-W.; Deng, B.; Antonietti, M.; Cölfen, H. *J. Phys. Chem. B* **2006**, *110*, 2988; (c) Zhang, J.; Liu, H.; Wang, Z.; Ming, N.; Li, Z.; Biris, A. S. *Adv. Funct. Mater.* **2007**, *17*, 3897.
22. (a) Greene, L. E.; Laq, M.; Goldberger, J.; Kim, F.; Johnson, J. C.; Zhang, Y.; Saykally, R. J.; Yang, P. *Angew. Chem. Int. Ed.* **2003**, *42*, 3031; (b) Hughes, W.; Wang, Z. L. *J. Am. Chem. Soc.* **2004**, *126*, 6703.

Chapter 2. Large-scale Synthesis of Perpendicular Side-Faceted One-Dimensional ZnO Nanocrystals

2.1. Introduction.

In recent years, a broad range of applications, ranging from photonic crystals,¹ photodetectors,² photodiodes,³ light-emitting diodes,⁴ varistors,⁵ and gas sensors,⁶ to solar cells,⁷ which is based on ZnO nanomaterials, has been reported due to its excellent chemical and thermal stability, and its specific optoelectronic and electrical property of being a II-VI semiconductor with a wide bandgap of 3.37 eV and a large exciton binding energy of 60 meV. As one-dimensional nanostructures are the deal system for studying the transport process in 1D confined objects, which are of benefit not only for understanding the fundamental phenomena in low dimensional systems, but also for developing new generation nanodivices with high performance.^{8,9} The synthesis of one-dimensional ZnO nanostructures has attracted considerable interest because of their promising applications in optics, optoelectronics, catalysis and piezoelectricity.^{9,10} One-dimensional ZnO nanostructures have been successfully fabricated by chemical vapor deposition (CVD),¹¹ thermal evaporation,⁹ molecular beam epitaxy (MBE),¹² and a high-temperature vapor transport process¹³ with the requirements of high-temperatures or special equipments. In addition, the preparations of one-dimensional ZnO nanostructures via wet chemical techniques, which includes microemulsion hydrothermal synthesis,¹⁴ direct deposition in aqueous solution,¹⁵ surfactant-assisted hydrothermal orientation growth,^{16, 17} and alcohol solution refluxing,^{18, 19} have been reported with their low growth temperatures and good feasibility for scale-up. As the recent researches suggested, in addition to size and dimension, the cross-section also a shape-effect on the properties of nanomaterials,²⁰

one-dimensional ZnO nanostructures with rectangular cross-sections have been tailored by thermal evaporation method^{9,21} and wet chemical methods¹⁷. Unfortunately, for the thermal evaporation method, ZnO nanobelts with uniformly narrow width have been reached rarely in the published works. Moreover, for the wet chemical methods, the cross-section control needs organic compounds as templates, and those ZnO nanostructures have wider widths which are over 50 nm, and the growth processes have been simply ascribed to template help or attachment-driven.¹⁷ Stimulated by our early work,¹⁹ our strategy to design one-dimensional ZnO nanostructures with perpendicular side-facets and varies aspects from cubes to rods, narrow wires (with diameter range down to 15 nm) and meso-, microcrystallites is based entirely on a wet chemical, bottom-up approach that synthesized, without template, from the theoretical modeling and experimental monitoring of the alcohol-oxide interfacial thermodynamics and kinetics of nucleation, growth, and aging processes. Furthermore, this technique has already been successfully demonstrated by the fabrication of large, one-dimensional growth of other kinds of one-dimensional nanomaterials in our further work.

2.2. Experiment

The synthesis was conducted by the solvothermal decomposition of a Zn(II) hydroxy complex with reagent grade chemicals. Experimental autoclaves, with 160 ml. teflon inside liner, were transfused with an alcoholic solution of zinc chloride (ZnCl_2 , 99.99%, Aldrich), zinc acetate dihydrate, $((\text{C}_2\text{H}_3\text{O}_2)_2\text{Zn}$, 98+%, Aldrich), sodium hydroxide (NaOH , 97%, Aldrich), methanol (CH_3OH , 98%, Aldrich) and ethanol ($\text{CH}_3\text{CH}_2\text{OH}$, 98%, Aldrich). After the solution was stirred for 30 min, white color slurry was appeared. Then the autoclaves were airproofed and heated at a constant temperature for several hours in a regular laboratory oven. After reactions,

the clear superstratum solutions were carefully removed, and the white color products were respectively washed by ethanol and water for several times to remove the unreacted chemicals, then the products were vacuum dried.

The crystal structure was determined with powder X-ray diffraction (XRD, Philips X'Pert-MPD system, Cu K α radiation, $\lambda = 1.54056 \text{ \AA}$) at a scanning rate of 0.02° per second for 2θ in the range from 5° to 80° . The morphology and compositional information of the product materials was obtained with transmission electron microscopy (TEM, JEOL, JEM-2010), high-resolution TEM, selected area electron diffraction and energy-dispersive X-ray spectroscopy (HRTEM/ED/EDS, HITACHI, H-7500), field emission scanning electron microscopy (FE-SEM, JEOL, JSM-6700FSEM).

2.3. Result and Discussion

To give an insight into the capability of controlling one-dimensional crystalline ZnO with perpendicular side-facets is over the width controlling. Moreover, to reach the low nanometer range, the design of one-dimensional, highly facet-oriented nanostructures, as well as different width and length range controlling of ZnO fabrication, is presented by following similar theoretical concepts. Due to the electronic configuration and ionic strength on the octahedral-tetrahedral equilibrium of the complex of Zn(II), the inherent diversity of facets energy and lack of ligand-field stabilization energy as well as the inability of alcohol to deprotonate divalent metal cations at ambient pressure, require the utilization of solvothermal conditions and neutralization in basic medium or chemical complexation to generate zinc oxide from zinc salts.²² The different surface energy of the crystal facets supplies a possibility of fabricating the perpendicular side-faceted one-dimensional ZnO nanostructure.^{23,24} Such facts substantially limit the electrostatic control of the

interfacial tension and nucleation free energy. Therefore, the easiest way to obtain smaller anisotropic nanoparticles of ZnO is using weaker polarity alcohol solvent, or to lower the overall concentration of the reagents, or at lower temperature.

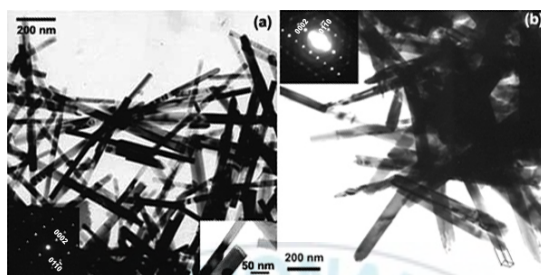


Figure 2-1. One-dimensional ZnO nanomaterials with different widths and their corresponding electron diffraction (ED) patterns: (a) 25 – 40 nm width range, and (b) 75 – 90 nm width range.

As expected, without surfactant as templates, single-crystalline one-dimensional ZnO nanostructures with the perpendicular side-facets, typically 25 to 40 nm wide, 15 nm thick and almost 500 nm to 1 μ m long, grew in 20 ml. methanol solution that contained 0.01 M zinc chloride and 0.1 M sodium hydroxide at 200 °C for 24 h (Figure 2-1(a)). And in Figure 2-1(b), 75 to 90 nm wide and 30 nm thick structures were yielded in 20 ml. ethanol solution containing 0.02 M zinc chloride and 0.15 M sodium hydroxide at 160 °C for 24 h. With same reaction parameters, this perpendicular side-faceted aspect was not observed in the ethanol solvent, which will be discussed later. Well-defined faces, i.e., polar facets (0002), non-polar facets {01-10} and the single crystalline characteristic can clearly be identified by the white color points arraying in the image of the electron diffraction (ED) pattern (Figure 2-1(a) and (b) inset). The rectangular cross-section can be confirmed by the enlarged image at the right bottom corner in Figure 2-1(a). The rougher ends with double or triple tips in Figure 2-1(b) hinted the different growth of crystal.

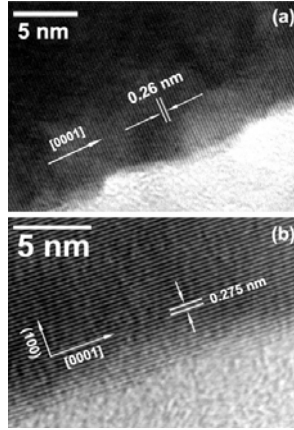


Figure 2-2. Corresponding HR-TEM images of the ZnO nanostructures in Figure 2-1(a) and (b), respectively.

In the enlarged HRTEM images, the smooth edges without amorphous shell of the one-dimensional ZnO nanostructures accord the Screw dislocation model very well. The interplanar spacing of the crystalline stripes is 0.26 nm and can be indexed to the (002) plane corresponding with the [0001] growth orientation in Figure 2-2(a), and 0.275 nm interplanar spacing of the (100) plane identifying the {01-10} side facets in Figure 2-2(b), respectively. In addition, both HR-TEM images are perfectly consistent with the electron diffraction patterns in Figure 2-1(a) and (b) insets on the single crystalline characters, polar growth orientation and the non-polar side-facets.

For the fabrication of one-dimensional nanostructures, it can be separated into two steps: (i) nucleation and (ii) crystal growth. In general, the minimum size of one-dimensional nanostructures is both dependent on nucleation thermodynamics and the growth kinetics (energy stability theory).^{25, 26} At the nucleation stage, the overall Gibbs free energy of formation of the cluster, ΔG_t , is given as the sum of the decrease in the Gibbs free energy of formation of the cluster lattice, ΔG_l , and the surface excess energy, ΔG_s :

$$\Delta G_t = \Delta G_l + \Delta G_s$$

As the plus valued ΔG_s , under the same ΔG_l value condition, the low energy facets such as non-polar facets $\{01-10\}$ and polar facets (0002) in zinc oxide crystal that have the preference to be formed firstly.²³ The selectable formation of different energy facets can be observed under a more moderate reaction condition, for example, in this paper, using lower polarity alcohol solvent as media to instead of water in solvothermal reactions.

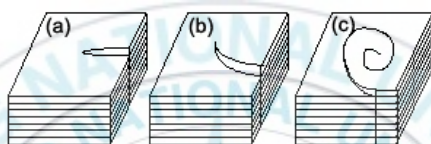


Figure 2-3. Screw dislocation model. (a) lattice defect, (b) and (c) propagation of screw.

As shown in Figure 2-3, in the model of Screw dislocation of crystal growth, the kink site (such as lattice defects, etc.) has the highest binding energy and is the most favorable position for the incorporation of a unit molecule from the solution phase, additionally, the angular velocity near the corner of the lattice defects is faster than that at the edge of the crystal. Therefore, the dislocation proceeds in a spiral form on the propagation of the step.²⁶ The model also suggested that once the smooth facets of the crystals has been formed, the spontaneously precipitating molecules stick on these surfaces differently. Thus the extending of the smooth low energy side-facets, the non-polar $\{01-10\}$ facets, can lead the oriented growth of the crystals into one-dimensional under a given reaction condition. In fact, our experimental results matched with the Screw dislocation theory perfectly with the smoothly perpendicular side-facets, the rough tips and planed bottoms and the uniform width and thickness along the entire length of the one-dimensional ZnO nanostructures.

Furthermore, this growth model might discover the real growth processes in a wide range of fabricating one-dimensional nanomaterials via a solvothermal process.

Generally, the increase in the degree of supersaturation and the increase in temperature usually cause an increase in the density of kink sites and in the roughness of the surface. The growth mechanism changes to adhesive growth, i.e., monomers which reach the surface are effectively incorporated into the crystal without surface diffusion.²⁶ Considering of the polarity for alcohol solvent in our experiments and the resulting white slurry before solvothermal reaction, monomer in the reactions should be zinc hydroxide. Therefore, with increased precursor concentration, in Figure 2-1(b), the rougher ends with double or triple tips on the one-dimensional ZnO structures were formed.

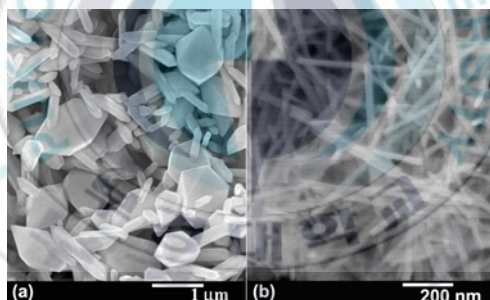


Figure 2-4. Products from ethanol solution at 200 °C, reacted for (a) 24 h, (b) 1 h.

The elongated structures character the kinetic control reactions. The monomer concentration can be indirectly controlled by changing the reactants with different hydrolyzing capability, the solvents with different polarity, the ratio between the reactants, and the reaction temperatures. For instance, because of the higher polarity, ethanol solvent can supply higher monomer concentration than methanol at same reaction condition. The higher monomer concentration can supply higher kinetic energy and chemical potential that will cause faster reaction rate. Thus, at 200 °C

with 0.01 M zinc chloride and 0.1 M sodium hydroxide, in the 20 ml. ethanol solution after 24 h, only large structures with two sharp ends can be observed (Figure 2-4(a)). And the products prepared with 1 h reaction under same reaction parameters shows a uniform aspect, as shown in Figure 2-4(b).

The different morphologies shown in Figure 2-4(a) and (b) respectively tallied with “1D to 2D ripening” and the further Ostwald ripening, and “1D growth” in the early stage which had been firstly reported by Peng et al.²⁷ At the early stage of reaction, high monomer concentration cause the growth focusing on the c-axis in the wurtzite structure and leading the “1D-growth” that produce the uniform one-dimensional structures in Figure 2-4(b). With the increasing reaction time, the monomer concentration drops to a certain level, the equal chemical potential in the bulk solution and of the entire surface atoms of the nanocrystal leads to a diffusion equilibrium on the interface. The monomers diffuse from the stagnant solution of the {0001} facets to the stagnant solution of the other facets. And when the monomer concentration is very low, the Ostwald ripening causes a “defocusing of size distribution” and produces the structures with very different size range as shown in Figure 2-4(a).

By controlling the reactants, the solvents, the reaction temperatures and time, the morphology of the perpendicular-side-faceted one-dimensional ZnO can be successfully displayed in a wide aspect range. In Figure 2-5, image (a) shows the one-dimensional ZnO with main diameters between 50 to 70 nm, which was yielded in an 20 ml. ethanol solution containing with 0.02 M ZnCl₂ and 0.2 M NaOH at 160 °C for 24 h. All the structures reveal their perpendicular side-facets with the flat bottoms and rough tips those are from the Screw dislocation growth. The strict control of the precipitation and dispersion conditions allows the interfacial free

energy of the system to be monitored. Therefore, without requirements of template, membrane, and surfactant to create anisotropic property or to control the growth orientation, the generation of well-defined and well-facet-oriented nanostructures within variable size and shape is allowed.

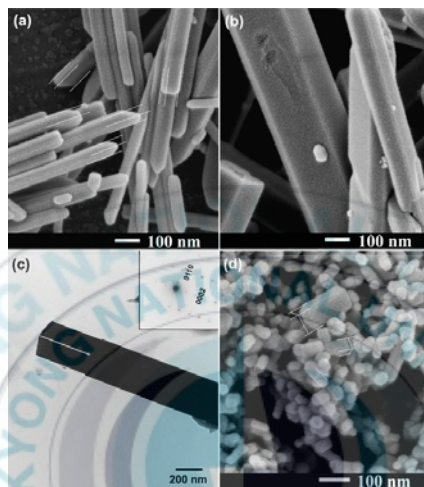


Figure 2-5. SEM and TEM images of variable ZnO nanostructures with perpendicular side-facets. (a) formed in ethanol solvent; (b) and (c) secondary grew in ethanol solvents; (d) secondary grew from nanoparticles to cubics.

With the control of ions releasing speed by using the low polarity alcohol solvents, micro-sized one-dimensional ZnO structures can be generated by increasing temperature or concentration of reactants, or a secondary growth under the same conditions. As shown in Figure 2-5(b) and (c), the ZnO structures secondarily formed in 20 ml. ethanol solutions containing with 0.005 M ZnCl_2 and 0.05 M NaOH, and 0.01 M ZnCl_2 and 0.1 M NaOH at 160 °C for 24 h. After the first time growth in the solution, the superstratum clear solution is carefully removed, and then the same precursor solution is injected into the reaction system and reacted under the same reaction condition. This process is named secondary growth in this article. Those materials were observed with their increased width and thickness, and the

remained perpendicular side-facets. Moreover, they are still single crystalline structures confirmed by the homologous electron diffraction pattern. Quantized zinc oxide nanoparticles²⁸ has been used for secondary growth formed cubes in an 20 ml. ethanol solution contain 0.005 M zinc chloride and 0.05 M sodium hydroxide (Figure 2-5(d)).

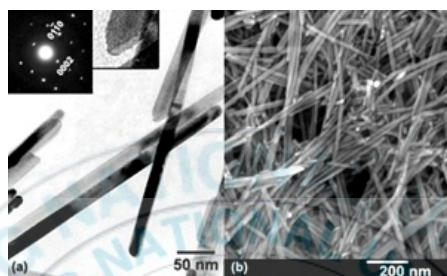


Figure 2-6. Narrow one-dimensional nanostructures with the perpendicular side-facets. (a) TEM image of the nanostructures and the corresponding electron diffraction pattern and an enlarged image of a tip; (b) the corresponding FE-SEM image.

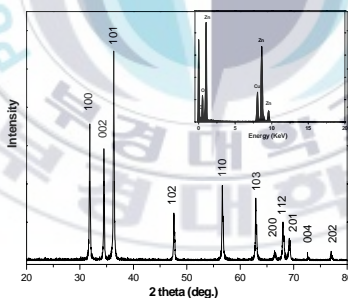


Figure 2-7. indexed XRD pattern and inset EDX analysis of the products.

In order to slow down the nucleation process, to form smaller perpendicular side-faceted nuclei with higher aspect ratio, zinc acetate had been used instead of zinc chloride as reactant. As expected, perpendicular side-faceted ZnO nanostructures, typically down to a narrowly 15 to 20 nm wide, 5 nm thick and up to 2 μ m long, grew in a 30 ml. ethanol solution that contained 0.01 M zinc acetate and

0.1 M sodium hydroxide at 100 °C for 24 h (Figure 2-6(a) and (b)). Well-defined faces, the single crystalline characteristic and the rectangular cross-section can clearly be identified by the electron diffraction (ED) pattern and enlarged image of the tip (Figure 2-6(a) inset). In Figure 2-7, the corresponding X-ray diffraction (XRD) spectrum of those nanostructures matches well with Bragg reflections of the typical crystal habit of wurtzite structured ZnO (P6₃mc, $a = 3.249 \text{ \AA}$, $c = 5.206 \text{ \AA}$, JCPDS No. 36-1451). The energy-dispersive X-ray spectroscopy (EDS) analysis of those nanostructures shows zinc and oxygen as the only detected elements with a ratio close to 1, except the copper from the copper grid, in Figure 2-7 inset.

2.4. Conclusion

In summary, one-dimensional ZnO with perpendicular side-facets can be easily synthesized in such an approach with more complex architecture over a large-scale. Low polarity alcohol, zinc salts with different hydrolyzing capabilities, varying reaction parameters have been knowledgeably used to control the reaction kinetic and limit the reaction to follow with the Screw dislocation model. The ultimate goal of such a study is to contribute to the grand challenges of nanotechnology, in other words, the low cost and large scale manufacturing of functional nanomaterials for realistic and practical applications.

References:

1. Chen, Y.; Bagnall, D.; Yao, T.; *Mater. Sci. Eng. B* **2000**, 75, 190.
2. Liang, S.; Sheng, H.; Liu, Y.; Hio, Z.; Lu, Y.; Shen, H. *J. Cryst. Growth* **2001**, 225, 110.
3. Lee, J. Y.; Choi, Y. S.; Kim, J. H.; Park, M. O.; Im, S. *Thin Solid Films* **2002**, 403, 553.

4. Saito, N.; Haneda, H.; Sekiguchi, T.; Ohashi, N.; Sakaguchi, I.; Koumoto, K. *Adv. Mater.* **2002**, *14*, 418.
5. Lin, Y.; Zhang, Z.; Tang, Z.; Yuan, F.; Li, J. *Adv. Mater. Opt. Electron.* **1999**, *9*, 205.
6. Golego, N.; Studenikin, S. A.; Cocivera, M. *J. Electrochem. Soc.* **2000**, *147*, 1592.
7. Keis, K.; Magnusson, E.; Lindstrom, H.; Lindquist, S. E.; Hagfeldt, A. *Sol. Energy* **2002**, *73*, 51.
8. (1) Cui, Y.; Wei, Q.; Park, H.; Lieber, C. M. *Science* **2001**, *293*, 1289; (2) Yang, H.; Yan, Y.; Liu, Y.; Zhang, F.; Zhang, R.; Meng, Y.; Li, M.; Xie, S.; Tu, B. and Zhao, D. *J. Phys. Chem. B* **2004**, *108*, 17320.
9. Pan, Z. W.; Dai, Z. R.; Wang, Z. L. *Science* **2001**, *291*, 1947;
10. (1) Gao, P. X.; Ding, Y.; Mai, W.; Hughes, W.; Lao, C.; Wang, Z. L. *Science* **2005**, *309*, 1700; (2) Wang, Y.; Zhang, L.; Meng, G.; Liang, C.; Wang, G. and Sun, S. *Chem. Commun.* **2001**, 2632.
11. (1) Wu, J. J.; Liu, S. C. *Adv. Mater.* **2002**, *14*, 215; (2) Liu, S. C. and Wu, J. J. *J. Mater. Chem.* **2002**, *12*, 3125.
12. Heo, Y. W.; Varadarajan, V.; Kaufman, M.; Kim, K.; Norton, D. P.; Ren, F.; Fleming, P. H. *Appl. Phys. Lett.* **2002**, *81*, 3046.
13. Lao, J. Y.; Wen, J. G.; Ren, Z. F. *Nano. Lett.* **2002**, *2*, 1287.
14. (1) Guo, L.; Ji, Y. L.; Xu, H.; Simon, P.; Wu, Z. *J. Am. Chem. Soc.* **2002**, *124*, 14865; (2) Zhang, J.; Sun, L. D.; Pan, H. Y.; Liao, C. S.; Yan, C. H. *New J. Chem.* **2002**, *26*, 33.
15. (1) Yamabi, S. and Imai, H. *J. Mater. Chem.* **2002**, *12*, 3773; (2) Gao, X. P.; Zheng, Z. F.; Zhu, H. Y.; Pan, G. L.; Bao, J. L.; Wu, F. and Song, D. Y. *Chem.*

- Commun.* **2004**, 1428.
16. (1) Liu, B. Zeng, H. C. *Langmuir* **2004**, 20, 4196; (3) Li, P.; Wei, Y.; Liu, H.; and Wang, X. *Chem. Commun.* **2004**, 2856.
17. (1) Zhang, X. Y.; Dai, J. Y.; Ong, H. C.; Wang, N.; Chan, H. L. W.; Choy, C. L. *Chem. Phys. Lett.* **2004**, 393, 17; (2) Zhang, D.-F.; Sun, L.-D.; Yin, J.-L.; Yan, C.-H. and Wang, R.-M. *J. Phys. Chem. B* **2005**, 109, 8786.
18. Pacholski, C. Kornowski, A.; Weller, H. *Angew. Chem. Int. Ed.* **2002**, 41, 1188;
19. Zhang, X. L.; Kim, Y. H and Kang, Y. S. *Current. Appl. Phys.* **2006**, in press.
20. Xiong, Q. H.; Wang, J. G.; Reese, O.; Voon, L. C. L. Y.; Eklund, P. C. *Nano Lett.* **2004**, 4, 1991.
21. (1) Wen, X.; Fang, Y.; Pang, Q.; Yang, C.; Wang, J.; Ge, W.; Wong, K. S. and Yang, S. *J. Phys. Chem. B* **2005**, 109, 15303; (2) Wei, Q.; Meng, G.; An, X.; Hao, Y. and Zhang, L. *Nanotechnology*, **2005**, 16, 2561.
22. Vayssieres, L. *Adv. Mater.* **2003**, 15, 464.
23. Wang, Z. L. *J. Phys.: Condens. Matter* **2004**, 16, R829.
24. Zhou, X.; Xie, Z.-X.; Jiang, Z.-Y.; Kuang, Q.; Zhang, S.-H.; Xu, T.; Huang, R.-B. and Zheng, L.-S. *Chem. Commun.*, **2005**, 5572.
25. Wang, C.-X.; Wang, B.; Yang, Y.-H. and Yang, G.-W. *J. Phys. Chem. B* **2005**, 109, 9966.
26. Ohtaki, H., *Crystallization Processes*, John Wiley & Sons Ltd, England, 1998.
27. (1) Peng, Z. A. and Peng X. *J. Am. Chem. Soc.* **2001**, 123, 1389; (2) Peng, Z. A. and Peng X. *J. Am. Chem. Soc.* **2002**, 124, 3343.
28. Spanhel, L. and Anderson, M. A. *J. Am. Chem. Soc.* **1991**, 113, 2826.

Chapter 3. Large-scale Synthesis of One-Dimensional Zinc Nickel Oxide Solid Solution

3.1. Introduction

One-dimensional wurtzite-structured ZnO nanomaterials have attracted extensive interest, because of the wide potential applications based on its optical and electric properties.¹ The direct band gap energy (3.37 eV) promises ZnO as an ideal candidate for low-voltage and short wavelength electro-optical devices in electronics, optoelectronics, photovoltaics and sensors. Fabricating one-dimensional nano-scaled crystal structures with designed electrical and optical properties is highly desired as beyond of the controlled shapes for application as sensors, field-emitters and spintronics.² Contemporaneously, on another research edge, led by the discovery of ferromagnetism in transition metal doped semiconductor, spintronics (spin-based electronics) has been deeply studied on both theories and experiments due to its enabling spin as well as the charge freedom of the carriers for new concept devices.³ To present as practical spintronics devices, the materials must exhibit ferromagnetic ordering at high temperature. In the quest for materials with a high magnetic transition temperature, transition metal doped ZnO has emerged as a attractive candidate based on theoretically predicted to be ferromagnetic at room temperature.^{3(b), 4} In fact, as one of the II-VI semiconductors, ZnO is optically transparent, and the direct wide band gap makes it an ideal candidate for the magneto optical devices.⁵ In addition, Dietl et al. suggested that $\text{Zn}_{1-x}\text{M}_x\text{O}$ ($M = \text{Mn}, \text{Fe}, \text{Ni}, \text{Co}$) exhibit a high transition temperature.^{3(b)}

Practically, this system has been experimentally studied, however, room temperature ferromagnetism has been reported in the vast majority of bulk materials, or thin films, or colloid, etc.⁶ ZnO based one-dimensional dilute magnetic solid

solutions (so-called dilute magnetic semiconductors, DMS) are of vital importance, since they not only play an important role as the building blocks of electronic and spintronic devices in the bottom-up milestone, but also provide excellent opportunities to study the effect of dimensionality and size on magnetism.⁷ To date, little work has been done on the fabrication of one-dimensional nanostructured $\text{Zn}_{1-x}\text{M}_x\text{O}$ through chemical vapor deposition (CVD) method, which has played as a superior since its quite effectiveness in producing a great amount of one-dimensional nanoscaled semiconductors.^{7, 8} Nevertheless, the CVD methods are evidently limited in homogeneous doping at the extreme vapor-phased experimental condition.

Solution-phased synthetic schemes for the producing $\text{Zn}_{1-x}\text{M}_x\text{O}$ isotropic quantum dots have been reported by Gamelin et al.⁹ Very recently, Yang et al. firstly reported a solution-phased method for fabrication $\text{Zn}_{1-x}\text{Co}_x\text{O}$ nanowire by thermal decomposition of zinc acetate and cobalt (II) acetate in refluxing trioctylamine at 310 °C.¹⁰ And Wong et al. reported a two-step solution-phased method for the synthesis of rod-shaped $\text{Zn}_{1-x}\text{Co}_x\text{O}$ by introducing pure ZnO seeds as nucleation centers.¹¹ Herein, following our early work on non-surfactant synthesizing one-dimensional ZnO nanomaterials,^{1(d)} we present a simple and facile method of large-scale synthesis of zinc oxide based one-dimensional solid solution with a series percentage of nickel dopant. Moreover, the synthetic process here also allows for the introduction of other transition metals, such as Co and Mn, etc.

3.2. Experimental Section

The synthesis of one-dimensional $\text{Zn}_{1-x}\text{Ni}_x\text{O}$ solid solution is based on an alcoholysis process originally developed for ZnO nanocrystal preparation by Kang et al.^{1(d)} $\text{Zn}_{1-x}\text{Ni}_x\text{O}$ nanorods with a series of percentage of nickel dopant were synthesized by similar procedures. In a typical $\text{Zn}_{1-x}\text{Ni}_x\text{O}$ nanorods synthesis, 4.95

mmol zinc acetate dihydrate ($(\text{C}_2\text{H}_3\text{O}_2)_2\text{Zn}\cdot 2\text{H}_2\text{O}$, 98+%, Aldrich) and 0.05 mmol nickel (II) acetate tetrahydrate ($(\text{C}_2\text{H}_3\text{O}_2)_2\text{Ni}\cdot 4\text{H}_2\text{O}$, 99.998%, Aldrich) were completely dissolved in 20 mL methanol (CH_3OH , >99.8%, Junsei). At 0 °C, 0.05 mol sodium hydroxide (NaOH , 97%, Junsei) was added into the above alcoholic solution with constant stirring. After about 30 min, virescent slurry formed, which was subsequently obturated in a 60 mL Teflon lined autoclave and kept at a constant temperature of 200 °C for 2 h in a regular laboratory oven. After the reaction systems cooling down, the products were washed by ethanol and water before froze-dry.

The crystal structure was determined with powder X-ray diffraction (XRD, Philips X'Pert-MPD system, $\text{Cu K}\alpha$ radiation, $\lambda = 1.54056 \text{ \AA}$) at a scanning rate of 0.02° per second for 2θ in the range from 15° to 80° . The morphology and compositional information of the product materials was obtained with transmission electron microscopy (TEM, HITACHI, H-7500), high-resolution TEM, selected area electron diffraction (HRTEM/ED, JEOL, JEM-2010), field emission scanning electron microscopy and energy-dispersive X-ray spectroscopy (FE-SEM/EDS, JEOL, JSM-6700FSEM). The magnetic properties of the obtained one-dimensional $\text{Zn}_{1-x}\text{Ni}_x\text{O}$ solid solution samples were investigated with SQUID (Quantum Design MPMS XL7).

3.3. Result and Discussion

The data of one-dimensional $\text{Zn}_{1-x}\text{Ni}_x\text{O}$ solid solution presented below correspond to one specific synthesis, but the electron microscopy characterizations of the products diluted with different nickel concentration have small variations in average size were similar. The products were dispersed in ethanol by sonication to prepare

samples for the measurements of TEM and SEM. Figure 3-1 shows transmission electron microscopy (TEM) and high-resolution TEM images of both $\text{Zn}_{1-x}\text{Ni}_x\text{O}$ and pure ZnO nanorods. In Figure 3-1 (a), there are no visible defects, second phase, or precipitation in $\text{Zn}_{1-x}\text{Ni}_x\text{O}$ nanorods compared with pure ZnO nanorods in Figure 3-1 (c). It suggests that the dopant is well-integrated into the lattice sites during the alcoholysis process. The diameter of the nanorods is statistically invariant regardless of nickel concentration. The average diameter of $\text{Zn}_{1-x}\text{Ni}_x\text{O}$ nanorods is 10 – 20 nm with length range from 0.2 to 1 μm , thus the $\text{Zn}_{1-x}\text{Ni}_x\text{O}$ nanorods have aspect ratios range of 10 – 100.

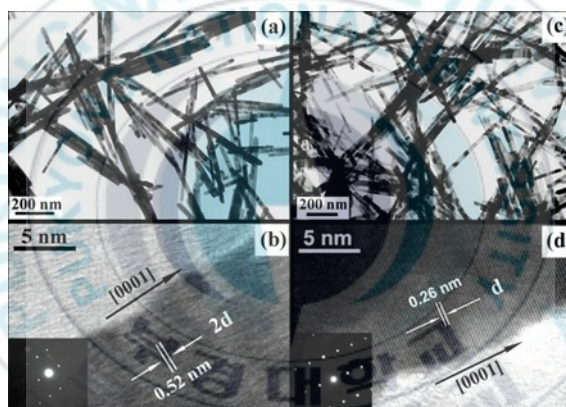


Figure 3-1. Electron microscopy characterization of the one-dimensional $\text{Zn}_{1-x}\text{Ni}_x\text{O}$ solid solution and pure ZnO nanorods. (a) TEM image of $\text{Zn}_{1-x}\text{Ni}_x\text{O}$ nanorods. (b) High-resolution TEM image of a single $\text{Zn}_{1-x}\text{Ni}_x\text{O}$ nanorod, with an accompanying electron diffraction pattern in the inset; similar images for pure ZnO nanorods are shown in (c) and (d).

More detailed structure information of the ZnO based nanorods was studied by high-resolution TEM (HRTEM) in conjunction with selected area electron diffraction (SAED) pattern. The crystal lattice morphology of the nanorods has been examined by high-resolution TEM. Both the lattice images, in Figure 3-1 (b) and (d), recorded along the nanorods clearly show the high crystallinity of the $\text{Zn}_{1-x}\text{Ni}_x\text{O}$ and pure ZnO nanorods with no visible line or planar defects, or amorphous shells on the

surfaces of the nanorods. The insets of Figure 3-1 (b) and (d) show the corresponding selected area electron diffraction (SAED) patterns from the same part of the nanorods shown in HR-TEM images (Figure 3-1 (b) and (d)). The clear linearly arranged patterns confirm that the $\text{Zn}_{1-x}\text{Ni}_x\text{O}$ nanorod has the wurtzite structure and there is no formation of a nickel precipitated as secondary phase. From the HR-TEM images and SAED patterns, it is seen that both kinds of the rods are single crystalline, with a growth direction along the c axis (indexes the $[0001]$ direction).

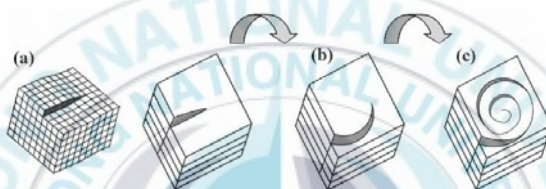


Figure 3-2. Screw dislocation model. (a) lattice defect, (b) and (c) propagation of screw.

The one-dimensional growth of pure ZnO nanorods has been reported previously in alcoholic solutions.^{1(d)} In the reported process, the one-dimensional growth was enabled by the Screw dislocation model of crystal growth, which can be simply presented in Figure 3-2. At the nucleation stage, the low-energy facets, such as the nonpolar facets $\{01-10\}$ and polar facets (0002) in wurtzite structure, have the preference to be formed first.¹² The kink site (ex. lattice defects, etc.) of the nuclei with the highest binding energy is the most favorable position for the incorporation of a unit molecule from the solution phase, and the angular velocity near the corner of the lattice defects is faster than that at the edge of the crystal. Thus, the dislocation proceeds in a spiral form in the propagation of the step, which results in the smooth side-facets of the crystals. Finally, the extending of the smooth low-energy side-facets, the $\{01-10\}$ facets of wurtzite structure, lead the oriented

growth into one-dimensional forms.^{1(d), 13} It is believed that the Screw dislocation model plays the similar role in fabrication of $\text{Zn}_{1-x}\text{Ni}_x\text{O}$ nanorods here, which formed the uniform diameters and single crystalline structures of the $\text{Zn}_{1-x}\text{Ni}_x\text{O}$ nanorods along their entire length on the c axis (the $[0001]$ growth direction).

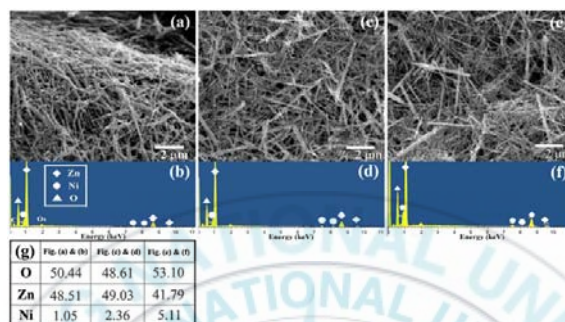


Figure 3-3. SEM images with the corresponding EDS spectra of $\text{Zn}_{1-x}\text{Ni}_x\text{O}$ nanorods with a series of percentage of nickel dopant (in the reactants): (a) and (b) 2.5%; (c) and (d) 5%; (e) and (f) 10% nickel doping; (g) The quantitative elemental distribution in atomic percentage determined from EDS analysis.

Figure 3-3 shows SEM images and the corresponding energy dispersive X-ray spectroscopy (EDS) of $\text{Zn}_{1-x}\text{Ni}_x\text{O}$ nanorods with various levels of nickel doping. The EDS spectra from Figure 3-3 (a), (c) and (e) are correspondingly displayed in Figure 3-3 (b), (d) and (f), respectively, and the quantitative elemental distribution in atomic percentage is tabled in Figure 3-3 (g). With consideration of the accuracy of the EDS analysis, we can conclude that there are $\sim 2.1\%$, $\sim 4.6\%$ and $\sim 10.9\%$ atomic ratio of nickel doping in the ZnO nanorods, respectively corresponding with the series levels of nickel acetate ranging from 2.5% to 5% and 10% in the reactants. The difference of nickel concentration between reactants and products is possibly caused by the formation of small oxide clusters of both ZnO and NiO, which did not precipitate out or, alternatively, the different dissolution ratios between ZnO and NiO clusters. Both of which were discarded in the purification steps.

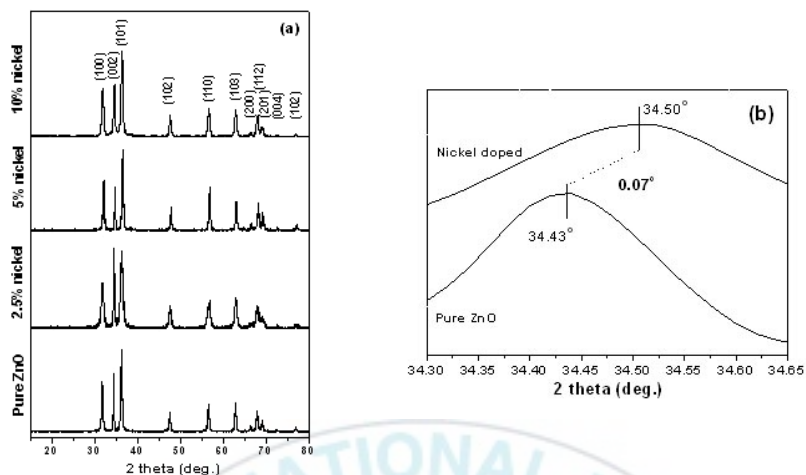


Figure 3-4. (a) XRD patterns of pure ZnO nanorods and $\text{Zn}_{1-x}\text{Ni}_x\text{O}$ nanorods with a series of percentage of nickel dopant (in the reactants). (b) High-resolution of (002) peak of pure ZnO and nickel doped ZnO nanorods.

Powder X-ray diffraction was used to characterize the structure of the products. Typical XRD patterns of $\text{Zn}_{1-x}\text{Ni}_x\text{O}$ nanorods with various levels of nickel doping are presented in Figure 3-4. In all cases, wurtzite is the only phase in existence that indicates the possible uniform doping throughout the nanorods. It should be noted that, even though no nickel clusters or other secondary phases were observed under the resolution limit of XRD, their existence cannot be completely excluded. However, the microstructure of the $\text{Zn}_{1-x}\text{Ni}_x\text{O}$ nanorods was examined by high-resolution TEM, all images show that the surfaces of the $\text{Zn}_{1-x}\text{Ni}_x\text{O}$ nanorods are rather smooth and clean and the uniform lattice throughout the entire lengths. Thus, nickel ions were uniformly doped into wurtzite ZnO by replacing the zinc sites. The small difference between the ionic radii of the tetrahedrally coordinated zinc (II) (0.74 Å) and the nickel (II) (0.69 Å) allows incorporation of Ni^{2+} into ZnO with only slight decrease in lattice parameters, which cause a shift of the ZnO (002) peak to a higher angle by about 0.07° (as shown in Figure 3-4 (b)). The similar

phenomenon, ZnO (002) peaks shifted to a lower angle due to the difference between the ionic radii of the tetrahedrally coordinated Mn (II) (0.80 Å) and Zn (II), was reported in Mn-doped ZnO nanowire by Lee et al.^{7(b)}

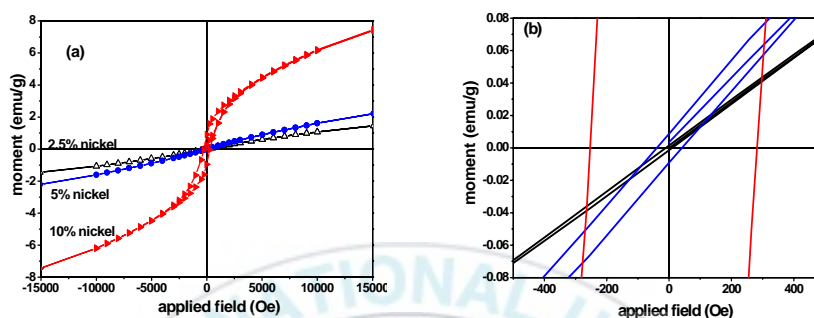


Figure 3-5. (a) 300 K magnetization of Zn_{1-x}Ni_xO nanorods with a series of percentage of nickel dopant in the reactants. (b) Enlarged central part of magnetization curve.

The magnetic properties of the Zn_{1-x}Ni_xO nanorods with various nickel doping levels were investigated on SQUID magnetometer. Figure 3-5 shows the magnetization (M) vs. magnetic field (H) measured at 300 K. The diamagnetic background of the sapphire substrate has been subtracted. Whereas paramagnetism dominates the magnetism of the Zn_{1-x}Ni_xO nanorods with low nickel doping levels, which is resulting in little detectable magnetization at 300 K, a clear hysteresis loop is observed in the ~10% of nickel doped Zn_{1-x}Ni_xO nanorods with a 300 K coercivity (H_c) of 259 Oe. It demonstrates that room-temperature ferromagnetic ordering exists in the one-dimensional ZnO solid solution with nickel solute. The physical origin of the ferromagnetic ordering from the dilute magnetic semiconductors is under arguments of whether the ferromagnetism is arising from the homogeneous magnetic doping or from magnetic precipitations.¹⁴ In our case, the single-phased XRD patterns, the slightly shifted ZnO (002) peak with nickel doping, and the well aligned lattice without any lattice distortion, and no nanoscale

phases have been observed in high-resolution TEM images. These confirm that nickel occupies zinc sites in $\text{Zn}_{1-x}\text{Ni}_x\text{O}$ nanorods. Therefore, the detected ferromagnetism here arises from the homogenous doping of nickel into ZnO crystal formed solid solutions.

3.4. Conclusion

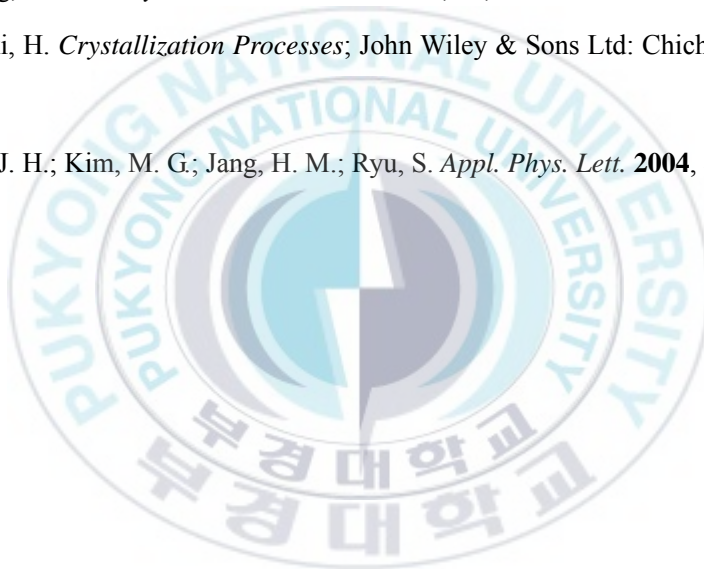
In conclusion, ZnO based solid solutions with different nickel concentration level were synthesized via a non-surfactant-assisted solvothermal method. The $\text{Zn}_{1-x}\text{Ni}_x\text{O}$ nanorods show ferromagnetic properties at room temperature. The structure analysis indicated that the $\text{Zn}_{1-x}\text{Ni}_x\text{O}$ nanorods are single crystalline. This suggests that the solid solution of nickel ions in ZnO nanorods plays a major role in producing the detected ferromagnetic behaviors. These $\text{Zn}_{1-x}\text{Ni}_x\text{O}$ nanorods offer applications in fundamental science and future nanoscale spintronic devices. Moreover, the economical and facile method presented here can be potentially applied in wide range of one-dimensional dilute magnetic semiconductors.

References

1. (a) Huang, M. H.; Mao, S.; Feick, H.; Yan, H.; Wu, Y.; Kind, H.; Weber, E.; Russo, R.; Yang, P. D. *Science* **2001**, 292, 1897; (b) Wang, Z. L.; Song, J. H. *Science* **2006**, 312, 242; (c) Minne, S. C.; Manalis, S. R.; Quate, C. F. *Appl. Phys. Lett.* **1995**, 67, 3918; (d) Zhang, X. L.; Kang, Y. S. *Inorg. Chem.* **2006**, 45, 4186.
2. (a) Choi, H. J.; Seong, H. K.; Chang, J. Y.; Lee, K.; Park, Y. J.; Kim, J. J.; Lee, S. K.; He, R. R.; Kuykendall, T.; Yang, P. D. *Adv. Mater.* **2005**, 17, 1351. (b) Zheng, G. F.; Lu, W.; Jin, S.; Lieber, C. M. *Adv. Mater.* **2004**, 16, 1890.
3. (a) Ohno, H. *Science* **1998**, 281, 951; (b) Dietl, T.; Ohno, H.; Matsukura, F.; Cibert, J.; Ferrand, D. *Science* **2000**, 287, 1019; (c) Archer, P. I.; Redovanovic, P.

- V.; Heald, S. M.; Gamelin, D. R. *J. Am. Chem. Soc.* **2005**, *127*, 14479; (d) Pan, D.; Wan, J.; Xu, G.; Lv, L.; Wu, Y.; Min, H.; Liu, J.; Wang, G. *J. Am. Chem. Soc.* **2006**, *128*, 12608.
4. Sato, K.; Katayama-Yoshida, H. *Phys. E* **2001**, *10*, 251.
5. (a) Chang, Y. Q.; Wang, D. B.; Luo, X. H.; Xu, X. Y.; Chen, X. H.; Li, L.; Chen, C. P.; Wang, R. M.; Yu, D. P. *Appl. Phys. Lett.* **2003**, *83*, 4020; (b) Pan, Z. W.; Wang, Z. L. *Science* **2001**, *291*, 1947.
6. (a) Sharma, P.; Gupta, A.; Rao, K. V.; Owens, F. J.; Sharma, R.; Ahuja, R.; Guillen, J. M. O.; Johansson, B.; Gehring, G. A. *Nat. Mater.* **2003**, *2*, 673; (b) Zhu, T.; Zhan, W. S.; Wang, W. G.; Xiao, J. Q. *Appl. Phys. Lett.* **2006**, *89*, 022508; (c) Nakayama, M.; Tanaka, H.; Masuko, K.; Fukushima, T.; Ashida, A.; Fujimura, N. *Appl. Phys. Lett.* **2006**, *88*, 241908; (d) Zhang, Y. B.; Liu, Q.; Sritharan, T.; Gan, C. L.; Li, S. *Appl. Phys. Lett.* **2006**, *89*, 042510; (e) Radovanovic, P. V.; Norberg, N. S.; McNally, K. E.; Gamelin, D. R. *J. Am. Chem. Soc.* **2002**, *124*, 15192; (f) Meron, T.; Markovich, G. *J. Phys. Chem. B* **2005**, *109*, 20232; (g) Deka, S. Pasricha, P.; Joy, P. A. *Chem. Mater.* **2004**, *16*, 1168.
7. (a) He, J. H.; Lao, C. B.; Chen, L. J.; Davidovic, D.; Wang, Z. L. *J. Am. Chem. Soc.* **2005**, *127*, 16376; (b) Baik, J. M.; Lee, J.-L. *Adv. Mater.* **2005**, *17*, 2745; (c) Liu, L. Q.; Xiang, B.; Zhang, X. Z.; Zhang, Y.; Yu, D. P. *Appl. Phys. Lett.* **2006**, *88*, 063104; (d) Philipose, U.; Nair, S. V.; Trudel, S.; Souza, C. F. de; Aouba, S.; Hill, R. H.; Ruda, H. E. *Appl. Phys. Lett.* **2006**, *88*, 263101.
8. Wu, J. - J.; Liu, S. - C.; Wang, M. - H. *Appl. Phys. Lett.* **2004**, *85*, 1027.

9. (a) Schwartz, D. A.; Norberg, N. S.; Nguyen, Q. P.; Parker, J. M.; Gamelin, D. R. *J. Am. Chem. Soc.* **2003**, *125*, 13205; (b) Schwartz, D. A.; Kittilstved, K. R.; Gamelin, D. R. *Appl. Phys. Lett.* **2004**, *85*, 1395.
10. Yuhas, B. D.; Zitoun, D. O.; Pauzauskie, P. J.; He, R.; Yang, P. *Angew. Chem. Int. Ed.* **2006**, *45*, 420.
11. Wang, H.; Wang, H. B.; Yang, F. J.; Chen, Y.; Zhang, C.; Yang, C. P.; Li, Q.; Wong, S. P. *Nanotechnology* **2006**, *17*, 4312.
12. Wang, Z. L. *J. Phys.: Condens. Matter* **2004**, *16*, R829.
13. Ohtaki, H. *Crystallization Processes*; John Wiley & Sons Ltd: Chichester, U.K., 1998.
14. Park, J. H.; Kim, M. G.; Jang, H. M.; Ryu, S. *Appl. Phys. Lett.* **2004**, *84*, 1338.



Chapter 4. Inorganic Cluster Synthesis and Characterization of Transition Metal-Doped ZnO Hollow Spheres

4.1. Introduction

Colloidal materials with uniformity in size, shape, composition and structure have attracted extraordinary attention in fields such as chemistry, physics, materials science, and biotechnology.¹ Colloidal spheres, in particular, represent a thermodynamically preferable state in terms of surface energy and thus are relatively easy to fabricate. Spherical colloidal materials made of metals or semiconductors, especially with porous structure and hollow interior, have been the topic of extensive research. Such materials exhibit highly desirable optical, electronic, magnetic, and catalytic properties that can be designed during the fabrication process.²⁻⁵ The applications range from robust catalysts, drug delivery, photonic devices, artificial cells, and active-material encapsulation to ionic intercalation and size-selective reactors.⁶⁻⁹ In general, it is difficult to grow colloidal spherical semiconductors with mesoscale dimensions because anisotropic growth is more favorable.² Heretofore, two kinds of template-directed synthetic methods have been reported with either hard⁶⁻¹² or soft¹³⁻¹⁶ templates for fabricating hollow structures. To generate the hollow interiors, further treatments such as calcinations or dissolution were needed to remove the templates. Recently, many efforts have been devoted to developing template-free methods in order to avoid these complex processes. Great challenges, however, still remain to prevent the incorporation of impurities and to achieve mesoscale size.¹⁷⁻¹⁹

In recent years, zinc oxide (ZnO)^{18,20-25} and zinc oxide based materials⁸ have been fabricated into hierarchical architectures to extend their potential applications.

Following the discovery of room-temperature ferromagnetic properties in dilute magnetic semiconductors (DMS) system that could lead to spintronics devices.^{29,30} Thus far, studies on zinc oxide based dilute magnetic semiconductors have involved syntheses of bulk materials,^{31,32} thin films,³³⁻³⁵ colloids and nanocrystals,³⁶⁻⁴⁰ and one-dimensional structures.⁴¹⁻⁴³ Spherical structures such as mesoscale spheres and hollow spheres have not yet been reported. In this paper, we demonstrate a template-free process for fabricating transition-metal-doped zinc oxide into mesoscale spheres and hollow spheres with porous shells, which contains initial aggregation and subsequent Ostwald ripening under solvothermal conditions. During the fabrication process, a low concentration of reactants was successfully employed to avoid anisotropic growth, leading to the formation of spherical aggregates.⁴³

4.2. Experiment

Materials: Zinc acetate dihydrate ($(\text{C}_2\text{H}_3\text{O}_2)_2\text{Zn}\cdot 2\text{H}_2\text{O}$, 98+%, Aldrich), nickel (II) acetate tetrahydrate ($(\text{C}_2\text{H}_3\text{O}_2)_2\text{Ni}\cdot 4\text{H}_2\text{O}$, 99.998%, Aldrich), cobalt (II) acetate tetrahydrate ($(\text{C}_2\text{H}_3\text{O}_2)_2\text{Co}\cdot 4\text{H}_2\text{O}$, >98%, Aldrich), lithium hydroxide monohydrate ($\text{LiOH}\cdot \text{H}_2\text{O}$, >98%, Junsei), methanol (CH_3OH , >99.8%, Hayman) were used as received without further purification.

Synthesis: In a typical template-free solvothermal process, 1.25 mmol mixed reactants (with zinc vs. nickel molar ratio of 9.0, a dopant concentration of 10%) were dissolved in 20 mL methanol with magnetic stirring for 1 h. Lithium hydroxide (0.05 g) was added into the above aqua solution with magnetic stirring and further sonicate dispersion at 0 °C. After being allowed to react at 200 °C for several hours in a Teflon-lined autoclave, the precipitates were carefully collected and washed with ethanol, then dried under vacuum. The synthesis of cobalt-doped ZnO hollow spheres was carried out through a modified process. A solution of 20 mL methanol

containing 1.25 mmol reactants with a stoichiometric percentage of cobalt ranging from 1 % to 10 % was reacted at 160 °C for the first 4 h and then at 200 °C for another 2 h.

Characterization: The crystal structure was determined with powder X-ray diffraction (XRD, Philips X'Pert-MPD system, Cu K α radiation, $\lambda = 1.54056 \text{ \AA}$) at a scanning rate of 0.02° per second for 2θ in the range from 10° to 80° . The spherical and hollow morphology and the composition of the products were analyzed with transmission electron microscopy (TEM, HITACHI, H-7500), high-resolution TEM and selected area electron diffraction (HR-TEM/SAED, JEOL, JEM-2010), field emission scanning electron microscopy and energy-dispersive X-ray spectroscopy (FE-SEM/EDS, JEOL, JSM-6700FSEM). The magnetic properties of the obtained hollow spherical samples were investigated with high sensitive magnetometer (SQUID, Quantum Design MPMS XL7).

4.3. Results and discussion

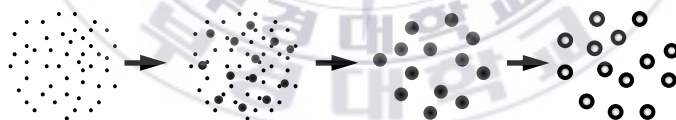


Figure 4-1. Schematic showing of the approach for the fabrication of nickel-doped zinc oxide hollow spheres.

Figure 4-1 schematically shows the functionalization of colloidal hollow spheres. The primary nuclei generated by hydrolysis subsequently aggregate into colloidal spheres, the succeeding localized Ostwald ripening process lead to the formation of cavities at the centre. This formation process has been elucidated by monitoring the morphology and crystallinity evolution by electron microscopy techniques. From

Figure 4-2(a) to (e), low resolution transmission electron microscopy (TEM) images show the morphology of products with increasing reaction time: (a) 1 h, (b) 1.5 h, (c) 2 h, (d) 4 h, and (e) 8 h. After the first 1 h solvothermal treatment, very small nanoseeds were obtained in Figure 4-2(a). In Figure 4-2(b), 1.5 h reaction generated both separated nanocrystallites and aggregated nanocrystallites. After another 30 min, approximately 200 nm diameter well-defined spheres with metastable aggregated nanocrystallites were formed that were easily broken by sonication in water (Figure 4-2(c)). Extending the reaction to 4 h resulted in a distinct increase in size (approximately 400 nm in Figure 4-2(d)), and a progressive increase in the crystallinity as increased intensity of XRD peaks. The inset of Figure 4-2(d) shows a field emission scanning electron microscopy (FE-SEM) image of a single sphere indicating the tightly aggregated nanocrystallites. With an associating redistribution of matter from the solid core, the growth of nanocrystallites produced hollow spheres within 8 h. In Figure 4-2(e), the contrasts in the TEM image reveal that vacancies formed at center of spheres (pointed out with white arrows). Moreover, porous shells were formed during the crystal growth process. The inset SEM image of a broken hollow sphere indicates the structure with a vacancy at the center and a polycrystalline porous shell. The corresponding selected area electron diffraction (SAED) rings are relatively sharp and perfectly index with polycrystalline zinc oxide. The SAED ring pattern of pure wurtzite zinc oxide indicated that the nickel dopant replaces zinc sites in the crystallite without any secondary phase generation. Lattice information of those hollow spheres from high resolution TEM (HR-TEM) images will be introduced later.

X-ray diffraction (XRD) pattern is shown in Figure 4-3. All peaks match well with wurtzite zinc oxide (JCPDS card no. 79-2205) without any secondary phase,

suggesting that the nickel (II) ions occupy the zinc (II) site in the wurtzite structure. It has been reported that transition-metal dopants were quantitatively excluded from the critical nuclei but were incorporated nearly isotropically during subsequent nanocrystalline growth.³⁷ The clear increase on peak intensity over time in Figure 4-3 demonstrates the increase of crystallite size. Calculated from X-ray line broadening using the Scherrer formula, $t = 0.9\lambda/\beta\cos\theta$,⁴⁴ the average sizes of nanocrystallites in the temporal samples are 11.3 nm for 2 h reaction, 12.5 nm for 4 h reaction and 15.2 nm for 8 h reaction.

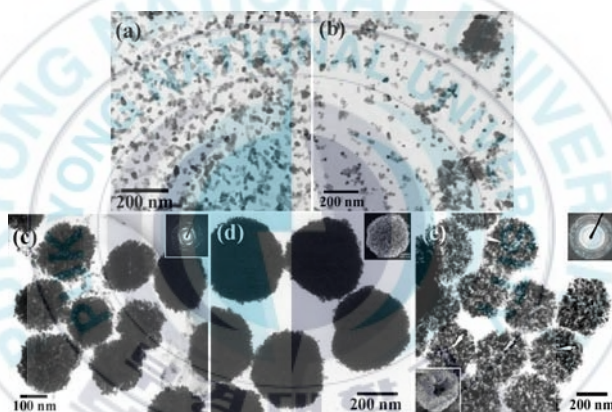


Figure 4-2. Time-dependent images of nickel-doped zinc oxide hollow spheres during the fabrication process: (a) 1 h; (b) 1.5 h; (c) 2 h (with corresponding SAED pattern as inset); (d) 4 h (with corresponding SEM image as inset); (e) 8 h (with corresponding SAED and SEM images as insets).

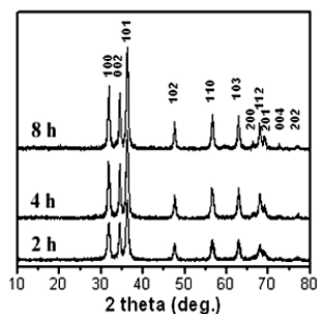


Figure 4-3. XRD patterns for the samples in Figure 4-2 (c), (d) and (e).

Figure 4-4 presents a large scale overview image with the obtained hollow spherical samples. The spheres with largely uniform in size and shape confirmed that the facile template-free synthesis process effectively generated spherical products with well confined size and structure. The rough shells are formed by aggregated small nanocrystallites. The contrasts in the TEM image of Figure 4-4(b) indicate the hollow interiors. The TEM image also shows worm-like pores with an average diameter of approximately 2 nm on the polycrystalline shell. The HR-TEM image in Figure 4-4(c) confirms the high crystallinity of the shell, and partially oriented attached nanocrystallites can be observed in some areas. In this figure, black arrows mark the double lattice spacing and indexed lattice fringe of d_{002} , d_{101} and d_{100} of wurtzite zinc oxide, which corroborate the XRD measurements.

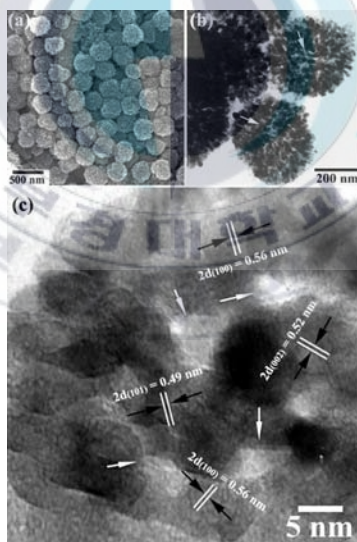


Figure 4-4. FE-SEM and TEM images of hollow spheres: (a) FE-SEM; (b) TEM images of two hollow spheres; (c) HR-TEM image of part of a single hollow sphere. White arrows point to pores.

The compositions of the samples were analyzed by energy dispersive X-ray spectroscopy (EDS) as shown in Figure 4-5. With 10% nickel dopant in the reactant,

the generated products have almost the same molar ratio of nickel (9.0~9.1%) that suggested effective and stable doping of the above described process. Following the interior hollowing process, the size of crystallites in the shells were also well controlled, allowing the fine-tuning of the optical band gaps of nickel-doped zinc oxide spheres and hollow spheres by means of particle size.

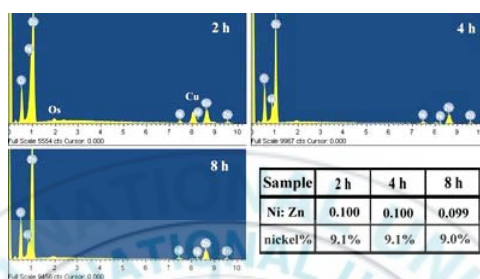


Figure 4-5. EDS measurements of temporal samples (at 200 °C for 2 h, 4 h and 8 h).

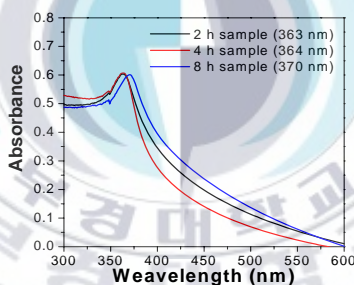


Figure 4-6. UV-visible absorption spectra of temporal samples (at 200 °C for 2 h, 4 h and 8 h). Peak positions are given in the graph legend.

To correlate crystallite size to the optical band gaps, UV-visible absorption spectra of the samples were measured (Figure 4-6). The absorption peak shows a red shift from 363 nm of samples after 2 h reaction, to 370 nm of samples after 8 h reaction, which was due to the nanocrystallites increase in size.⁴⁵ This result is indicative of the Ostwald ripening process (explained below), as the notable increase of the intensity of the XRD peaks. In addition, we carried out a series of nickel doping levels using the same synthetic process. In Figure 4-7, all XRD patterns from

these samples accurately match the pattern for wurtzite zinc oxide, indicating that the dopant is well-integrated into the lattice by taking the place of zinc.

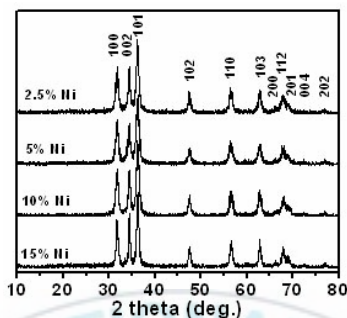


Figure 4-7. XRD patterns of samples with a series of doping levels. Each sample is labeled by the nickel percentage in the reactants. Only wurtzite zinc oxide phase can be confirmed. No other phase, such as nickel hydroxide or nickel oxide, can be detected.

The above results highlight a facile, template-free solvothermal process for the formation of uniform mesoscale hollow spheres. To avoid the large-scale anisotropic growth of crystals, reactions were carried out with low monomer concentration that could be controlled by using a low concentration of reactants. Thus, at the beginning of the reaction, hydrolysis of the zinc and nickel precursors generates primary nuclei that subsequently generate nanoparticles. The fresh crystalline nanoparticles with large exposed surface are unstable and tend to aggregate and form metastable spheres, driven by the minimization of the interfacial energy.^{46,47} In the surrounding solution, supersaturation falls with prolonged reaction that exhibits various packing densities along the radial direction, and an ultrathin shell of a less-soluble crystalline phase forms.⁴⁸ The highly soluble amorphous core with highest zinc concentration remains in nonequilibrium with the surrounding solution, which makes the core of sphere has the fastest erosion rate. The alkaline environment and gas-liquid equilibrium in the autoclave is the key factor to make the aggregated spheres erode

from the core to the outside.⁴⁹ During the crystal growth process, therefore, the core dissolves due to localized Ostwald ripening. Ostwald ripening involves the growth of larger crystals that have low solubility from those of smaller size with higher solubility.^{50,51} Hollow interiors are generated in this manner.

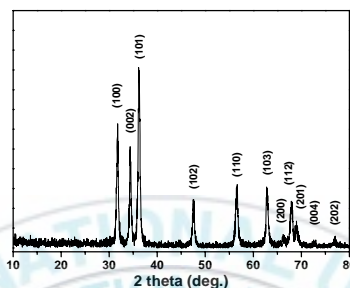


Figure 4-8. 300 K magnetization of Ni-doped ZnO hollow spheres synthesized from precursors containing different percentages of nickel dopant. The inset: temperature dependence of the magnetic moment.

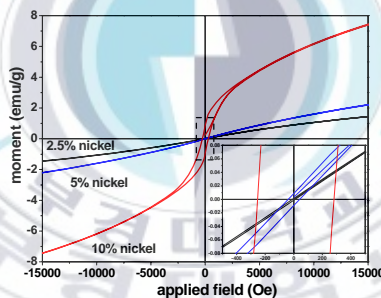


Figure 4-9. 300 K magnetization of Zn_{1-x}Ni_xO nanorods with a series of percentage of nickel dopant in the reactants.⁴³

Figure 4-8 presents the 300 K magnetization data of obtained hollow spheres containing nickel dopant percentage of 9.0 % (in black), 17.6% (in blue) and 27.1 % (in red). The blue and red curves have clear hysteresis loops with coercive fields of approximately 16 Oe with remanence of 0.14×10^{-3} emu/g (blue curve) and 0.31×10^{-3} emu/g (red curve). No T_c was noticed within the studied temperature range, but a gradual decrease in magnetization was observed for increasing temperature.

Similar phenomena were reported in other DMS materials.⁵²⁻⁵⁴ It is well known that not only the material composition but also the long-range order of the crystalline lattice can influence functionality of obtained materials. In contrast to the one-dimensional nickel-doped zinc oxide we have recently studied (Figure 4-9),⁴³ the poor magnetic properties of the hollow spheres indicate that there was no long-range magnetic ordering in the obtained hollow spheres. Aggregation likely generates many defects at interfaces between adjacent nanocrystals; these defects may induce n-type character.⁵⁵ Ferromagnetism has been reported in reaction-limited aggregated nanocrystalline nickel doped zinc oxide, while paramagnetism has been observed in the freestanding crystals.⁵⁶ The combined effects of increased domain volumes and the introduction of n-type lattice defects with reaction-limited aggregation result in the appearance of ferromagnetism. Therefore, the poor magnetization in nickel-doped zinc oxide hollow spheres can be attributed to the relatively fast aggregation and the accompanying introduction of n-type lattice defects.

A modified synthetic process with two reaction periods at different temperatures was used to fabricate cobalt-doped zinc oxide hollow spheres. The reports of H. C. Zeng's group⁵⁷ proved that high process temperature was suitable for rapid core evacuation in the fabrication of CuO hollow spheres. For fabrication of cobalt-doped zinc oxide hollow spheres, the reaction temperature was first increased to 160 °C for a 4 h reaction, then the temperature was increased to 200 °C for a 2 h reaction. TEM and FE-SEM images (Figure 4-10) represent the morphology of products, with approximately 1% cobalt dopant in precursors. Well-defined hollow spheres with approximately 200 nm diameter were observed. The contrast between the vacancies at the centers and the high density shells illustrates the hollow structures. This

structure can also be seen in the inset SEM image of a broken hollow sphere (Figure 4-10(a)). In the corresponding XRD pattern (Figure 4-11) all peaks match well with wurtzite zinc oxide (JCPDS card no. 79-2205).

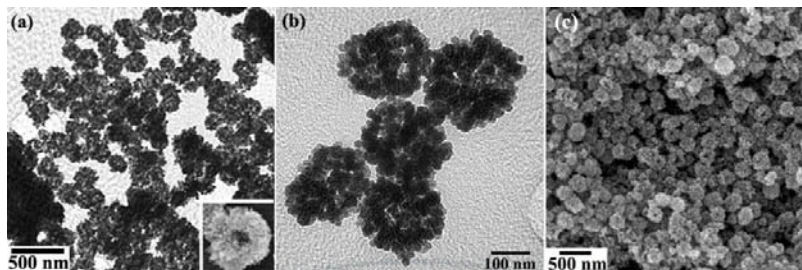


Figure 4-10. Cobalt-doped ZnO hollow spheres: (a) TEM image with a single broken hollow sphere shown in the inset, (b) TEM images, (c) FE-SEM image and (d) XRD pattern.

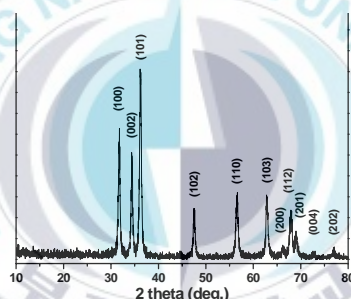


Figure 4-11. XRD pattern of the samples in Figure 6.

Figure 4-12 shows the magnetic hysteresis loop measured at 300 K for the sample of Figure 4-4. Interestingly, despite the low doping level, the cobalt-doped zinc oxide hollow spheres exhibit a robust coercivity (H_c) of approximately 100 Oe. The coercivity almost disappears at samples with higher cobalt doping levels (Figure 4-13). As for nickel-doped zinc oxide hollow spheres, a gradual decrease in magnetization is observed with responding to increasing temperature, but no T_c is detected within the considered temperature range (Figure 4-12, inset). Unlike previous reports of cobalt-doped zinc oxide nanocrystals,^{39,40} the hysteresis loop

only appears at the magnetization of this low doping level sample.

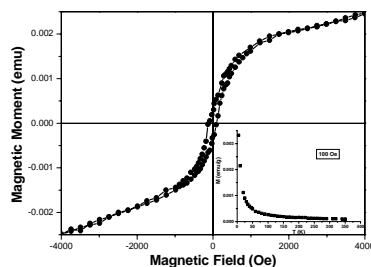


Figure 4-12. 300 K magnetization of Co-doped ZnO hollow spheres. The inset: temperature dependence of the magnetic moment.

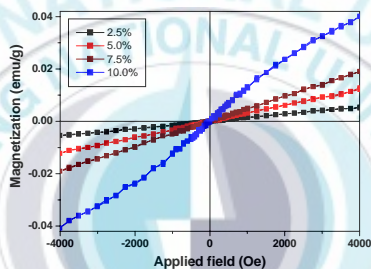


Figure 4-13. 300 K magnetization of cobalt-doped ZnO hollow spheres (with a series of percentage of cobalt dopant in the precursors).

4.4. Conclusion

In this work, nickel- and cobalt-doped zinc oxide hollow spheres have been produced through a facile, template-free synthesis by introducing nickel (II) cations and cobalt (II) cations into the zinc ion starting solution. A robust room-temperature ferromagnetism was found in cobalt-doped zinc oxide hollow spheres, while nickel-doped zinc oxide hollow spheres exhibited only weak ferromagnetism at 300 K. This solution route, with its morphologically confined processes of spontaneous aggregation and localized Ostwald ripening, shows promise as an industrially easy and environmental benign method.

References

1. Russel, W. B.; Saville, D. A.; Schowalter, W. R. *Colloidal Dispersions*, in Cambridge Monographs on Mechanics, Cambridge University Press, New York **1989**.
2. Jeong, U.; Wang, Y.; Ibisate, M.; Xia, Y. *Adv. Funct. Mater.* **2005**, *15*, 1907;
3. Wang, Y.; Cai, L., Xia, Y. *Adv. Mater.* **2005**, *17*, 473;
4. Yang, H. G.; Zeng, H. C. *Angew. Chem. Int. Ed.* **2004**, *43*, 5206;
5. Zhou, H.; Fan, T.; Zhang, D.; Gu, Q. Ogawa, H. *Chem. Mater.* **2007**, *19*, 2144.
6. Caruso, F.; Caruso, R. A.; Möhwald, H. *Science*, **1998**, *282*, 1111;
7. Göltner, C. G. *Angew. Chem. Int. Ed.* **1999**, *38*, 3155;
8. Sun, Y.; Xia, Y. *Science*, **2002**, *298*, 2716;
9. Dinsmore, A. D.; Hsu, M. F.; Nikolaides, M. G.; Marquez, M.; Bausch, A. R.; Weitz, D. A. *Science*, **2002**, *298*, 1006.
10. Caruso, R. A.; Schattka, J. H.; Greiner, A. *Adv. Mater.* **2001**, *13*, 1577;
11. Yang, Z.; Niu, Z.; Lu, Y.; Hu, Z.; Han, C. C. *Angew. Chem. Int. Ed.* **2003**, *42*, 1943;
12. Kobayashi, S.; Hamasaki, N.; Suzuki, M.; Kimura, M.; Shirai, H.; Hanabusa, K. *J. Am. Chem. Soc.* **2002**, *124*, 6550.
13. Blin, J. L.; Léonard, A.; Yan, Z. Y.; Gigot, L.; Vantomme, A.; Cheetham, A. K.; Su, B. L. *Angew. Chem. Int. Ed.* **2003**, *42*, 2872;
14. Peng, Q.; Dong, Y.; Li, Y. *Angew. Chem. Int. Ed.* **2003**, *42*, 3027;
15. He, T.; Chen, D.; Jiao, X.; Wang, Y. *Adv. Mater.* **2006**, *18*, 1078;
16. Qiao, R.; Zhang, X. L.; Qiu, R.; Li, Y.; Kang, Y. S. *J. Phys. Chem. C* **2007**, *111*, 2426.

17. Nakashima, T.; Kimizuka, N. *J. Am. Chem. Soc.* **2003**, *125*, 6386;
18. Liu, B.; Zeng, H. C. *J. Am. Chem. Soc.* **2004**, *126*, 16744;
19. Liu, B.; Zeng, H. C. *J. Am. Chem. Soc.* **2004**, *126*, 8124.
20. Huang, M. H.; Mao, S.; Feick, H.; Yan, H.; Wu, Y.; Kind, H.; Weber, E.; Russo, R.; Yang, P. D. *Science* **2001**, *292*, 1897;
21. Kong, X. Y.; Ding, Y.; Yang, R. S.; Wang, Z. L. *Science* **2004**, *303*, 1348;
22. Gao, P. X., Wang, Z. L. *J. Am. Chem. Soc.* **2003**, *125*, 11299;
23. Gao, P. X., Wang, Z. L. *J. Phys. Chem.* **2002**, *106*, 12653;
24. Yao, K. X.; Zeng, H. C. *J. Phys. Chem. B* **2006**, *110*, 14736;
25. Zhang, X. L.; Kang, Y. S. *Inorg. Chem.* **2006**, *45*, 4186.
26. Wang, W.-W.; Zhu, Y.-J.; Yang, L.-X. *Adv. Funct. Mater.* **2007**, *17*, 59;
27. Wang, Y. S.; Thomas, P. J.; O'Brien, P. J. *Phys. Chem. B* **2006**, *110*, 21412;
28. Duan, L.; Lin, B.; Zhang, W.; Zhong, S.; Fu, Z. *Appl. Phys. Lett.* **2006**, *88*, 232110.
29. Ohno, H. *Science* **1998**, *281*, 951;
30. Dietl, T.; Ohno, H.; Matsukura, F.; Cibert, J.; Ferrand, D. *Science* **2000**, *287*, 1019;
31. Sharma, P.; Gupta, A.; Rao, K. V.; Owens, F. J.; Sharma, R.; Ahuja, R.; Guillen, J. M. O.; Johansson, B.; Gehring, G. A. *Nat. Mater.* **2003**, *2*, 673;
32. Zhu, T.; Zhan, W. S.; Wang, W. G.; Xiao, J. Q. *Appl. Phys. Lett.* **2006**, *89*, 022508.
33. Schwartz, D. A.; Kittilstved, K. R.; Gamelin, D. R. *Appl. Phys. Lett.* **2004**, *85*, 1395;

34. Khare, N.; Kappers, M. J.; Wei, M.; Blamire, M. G.; MacManus-Driscoll, J. L. *Adv. Mater.* **2006**, *18*, 1449;
35. Nakayama, M.; Tanaka, H.; Masuko, K.; Fukushima, T.; Ashida, A.; Fujimura, N. *Appl. Phys. Lett.* **2006**, *88*, 241908.
36. Radovanovic, P. V.; Norberg, N. S.; McNally, K. E.; Gamelin, D. R. *J. Am. Chem. Soc.* **2002**, *124*, 15192;
37. Schwartz, D. A.; Norberg, N. S.; Nguyen, Q. P.; Parker, J. M.; Gamelin, D. R. *J. Am. Chem. Soc.* **2003**, *125*, 13205;
38. Meron, T.; Markovich, G. *J. Phys. Chem. B* **2005**, *109*, 20232;
39. Deka, S.; Pasricha, P.; Joy, P. A. *Chem. Mater.* **2004**, *16*, 1168;
40. Wang, X.; Xu, J.; Zhang, B.; Yu, H.; Wang, J.; Zhang, X.; Yu, J.; Li, Q. *Adv. Mater.* **2006**, *18*, 2476.
41. He, J. H.; Lao, C. S.; Chen, L. J.; Davidovic, D.; Wang, Z. L. *J. Am. Chem. Soc.* **2005**, *127*, 16376;
42. Yuhas, B. D.; Zitoun, D. O.; Pauzauskie, P. J.; He, R.; Yang, P. *Angew. Chem. Int. Ed.* **2006**, *45*, 420;
43. Zhang, X. L.; Qiao, R.; Qiu, R.; Li, Y.; Kang, Y. S. *J. Phys. Chem. A* **2007**, *111*, 4195.
44. Cullity, B. D. *Elements of X-Ray Diffraction*, 2nd ed.; Addison-Wesley Publishing Company, Inc. 1978, pp. 284.
45. Meulenkaamp, E. A. *J. Phys. Chem. B* **1998**, *102*, 5566.
46. Wu, C.; Xie, Y.; Lei, L.; Hu, S.; OuYang, C. *Adv. Mater.* **2006**, *18*, 1727.
47. Zhu, L.-P.; Xiao, H.-M.; Zhang, W.-D.; Yang, G.; Fu, S.-Y. *Crystal Growth & Design* **2008**, *8*, 957.

48. Yu, J.; Guo, H.; Davis, S. A.; Mann, S. *Adv. Funct. Mater.* **2006**, *16*, 2035.
49. Chen, Z.; Gao, L. *Crystal Growth & Design* **2008**, *8*, 460.
50. Ostwald, W. Z. *Phys. Chem.* **1897**, *22*, 289;
51. Ostwald, W. Z. *Phys. Chem.* **1900**, *34*, 495.
52. Wang, H.; Wang, H. B.; Yang, F. J.; Chen, Y.; Zhang, C.; Yang, C. P.; Li, Q.; Wong, S. P. *Nanotechnology*, **2006**, *17*, 4312;
53. Kim, S. S.; Moon, J. H.; Lee, B.-T.; Song, O. S.; Je, J. H. *J. Appl. Phys.* **2004**, *95*, 454;
54. Choi, H. J.; Seong, H. K.; Chang, J.; Lee, K. I.; Park, Y. J.; Kim, J. J.; Lee, S. K.; He, R.; Kuykendall, T.; Yang, P. *Adv. Mater.* **2005**, *17*, 1351.
55. Zhang, S. B.; Wei, S.-H.; Zunger, A. *Phys. Rev. B* **2001**, *63*, 075205.
56. Radovanovic, P. V.; Gamelin, D. R. *Phys. Rev. Lett.* **2003**, *91*, 157202.
57. Chang, Y.; Teo, J. J.; Zeng, H. C. *Langmuir*, **2005**, *21*, 1074.

Chapter 5. Surfactant-Directed Fabrication of ZnO with Tunable Morphology

5.1. Introduction

The optical, electronic and catalytic responses of a material depend on its particular size, shape, component, and local dielectric environment.¹ In modern materials science, fabrication of size- and shape-controlled materials is one of the most important techniques in controlling their chemical and physical properties.² Zinc oxide, a direct band gap semiconductor with a large bandgap of 3.37 eV and a large exciton binding energy of 60 meV, is a candidate of various applications such as room-temperature UV lasers,³ light-emitting diodes,⁴ solar cells,⁵ photoelectronics,⁶ and sensors.⁷ As a polar crystal, ZnO can be described as a number of positively charged (0001) planes rich in Zn^{2+} ions and negatively charged (000-1) planes rich in O^{2-} ions alternatingly stacked along the c axis. Therefore, the positive polar (0001) surfaces and the negative polar (000-1) surface can have different self-catalysis properties.⁸ However, the spontaneous polarization along the c axis leads to the common formation of one-dimensional (1D) structures due to electrostatic interaction, and the large polar surface is generally energetically unfavorable.⁹

Among the developed synthetic methods, solid vapor phase (SVP) approaches have been used for fabricating a diversity of nano- or micro-scaled nanostructures at high temperature with its simplicity of process and high-quality of products.¹⁰ However, SVP approaches have major limitation in low yield. Solution phase synthetic approaches by thermal treatment of the reactant in different solvents media, may be the most simple and effective way to prepare sufficiently crystallized materials at relatively low temperatures, while exempted from further calcinations.

Besides this, the benefits of a utilizing solution-based method have also involved the considerable influence of reaction species on the final size and morphology of the as-synthesized samples on a large scale.¹¹ Recent reports demonstrated that large polar surface of ZnO can be generated when the surface charge is compensated by using polymers and surfactants as passivation agents.¹² Micelles formed by surfactants can have various shapes from spheres, rods, ellipsoids, to disks, and even much more complex structures by adjusting experimental parameters. Therefore, size- and shape controlled nano- or microstructures can be fabricated through solution phase synthesis.¹³ Here we demonstrate a facile rational surfactant-directed morphology control on hybrid ZnO materials in an environmental benign alcohol-water reaction medium. ZnO hybrid materials with diverse shapes ranging from mushroom-like, double hemi-spheres, dumbbell, to hexagonal bi-layer disks and flower-like aggregation of sheets, can be easily prepared on a large scale.

5.2. Experiment

Materials: Zinc nitrate hexahydrate ($\text{Zn}(\text{NO}_3)_2 \cdot 6\text{H}_2\text{O}$, analytic reagent, 95%, Junsei), sodium dodecylbenzenesulfonate ($\text{CH}_3(\text{CH}_2)_{11}\text{C}_6\text{H}_4\text{SO}_3\text{Na}$, SDBS, technical grade, Aldrich), sodium hydroxide (NaOH , analytic reagent, >93%, Junsei), ethanol ($\text{CH}_3\text{CH}_2\text{OH}$, >99.9%, Hayman) were used as received without further purification.

Synthesis: In typical synthesis, a specific amount of zinc nitrate, SDBS and sodium hydroxide were added into 45 mL ethanol water solution with vigorous stirring over 2 h. Then the reaction mixture was transferred into a Teflon-lined autoclave and kept at a constant temperature for several hours. The precipitates were collected and washed with deionized water, then dried under vacuum.

Characterization: The crystal structure was determined with powder X-ray

diffraction (XRD, Philips X'Pert-MPD system, Cu K α radiation, $\lambda = 1.54056 \text{ \AA}$) at a scanning rate of 0.02° per second for 2θ in the range from 10° to 80° . The morphology and compositional information of the product materials was obtained with transmission electron microscopy (TEM, HITACHI, H-7500), high-resolution TEM, selected area electron diffraction (HRTEM/ED, JEOL, JEM-2010), field emission scanning electron microscopy and energy- dispersive X-ray spectroscopy (FE-SEM/EDS, JEOL, JSM-6700FSEM).

5.3. Results and discussion

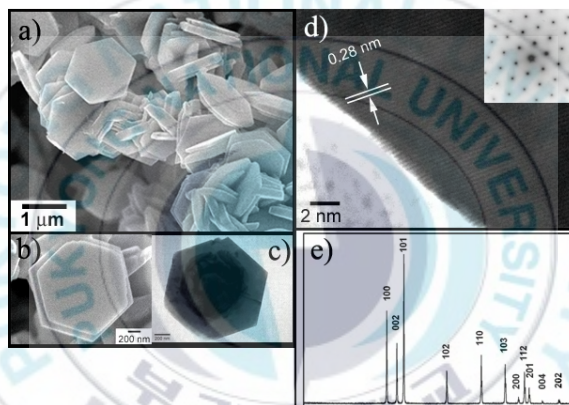


Figure 5-1. a) FE-SEM image of as-synthesized ZnO hexagonal disks. b), c) Enlarged SEM image and TEM image display detailed structures of hexagonal disks. d) HR-TEM image and SAED pattern (inset) of the sample in c). e) A corresponding XRD pattern of the same sample.

The ZnO hexagonal bi-layer disks were synthesized by a solution phase approach. In typical procedure, a novel two phase system – water/ethanol system – was designed, which is different from the conventional water/oil systems by means of its facile producing and non-environmental pollution.^{12, 14} Then the ZnO disks subsequently grow in microreactors formed with surfactant – sodium dodecylbenzenesulfonate (SDBS). Figure 5-1a) shows a typical field emission scanning electron microscopy (FE-SEM) image of ZnO samples synthesized in an ethanol solution containing 9.6 mmol SDBS, 2.4 mmol Zn(NO₃)₂, 3.6 mmol NaOH

and 3 mL deionized water with a reaction process at 90 °C for first 4 h and 180 °C for another 4 h. The as-synthesized product is pure and uniform, and dominated by hexagonal bi-layer disks with uniform size and well-defined shape. The disks are 1–1.5 μm in diameter and 50–200 nm thick. Enlarged scanning electron microscopy (SEM) and transmission electron microscopy (TEM) images show single disks with bi-layer structure (Figure 5-1b) and c)). The contrast in TEM image reveals a second layer with small diameter behind the first hexagonal disk. A high-resolution transmission electron microscopy (HR-TEM) image and the corresponding selected area electron diffraction (SAED) pattern obtained from a single disk with the electron beam perpendicular to the hexagonal facet. The lattice spacing of 0.28 nm indexes lattice fringe of d_{100} of wurtzite zinc oxide. The diffraction spots of the SAED pattern can be indexed into the diffraction spots of [000-1] zone of the wurtzite structure, which demonstrates the top and bottom surface of the bi-layer disks are the $\pm(0001)$ plane and the side surfaces parallel to the c -axis are the $\pm\{01-10\}$ planes. In Figure 5-1.c), the corresponding X-ray diffraction (XRD) patterns match well with a pure hexagonal wurtzite structure ($P6_3mc$, $a = 3.2501\text{\AA}$, $c = 5.2071\text{\AA}$).

The ethanol solution reaction system was studied by monitoring the influences of surfactant amount, water volume, NaOH amount and reaction temperature through the morphology evolution of products recorded by microscopy technique. While without water addition and with constant amount of zinc nitrate, the morphology of products changes slightly from hazelnut-like to mushroom-like structures, with a smooth cap and a rough bottom (Figure 5-2). With SDBS and Zn^{2+} ratio of 1.0, the products have hazelnut-like morphology with a sharp cap part as shown in Figure 5-2a). Increasing the ratio to 2.0, in Figure 5-2b), the hemispherical top part appears.

Further increase of SDBS makes the size decreasing on the bottom part of products as shown in Figure 5-2c) and d). Interestingly, with SDBS vs. Zn^{2+} ratio of 4.0, the products (Figure 5-2e) and f)) present a regular hemispherical part and a hexagonal step (or a hexagonal step with hexagonal concavity around it).

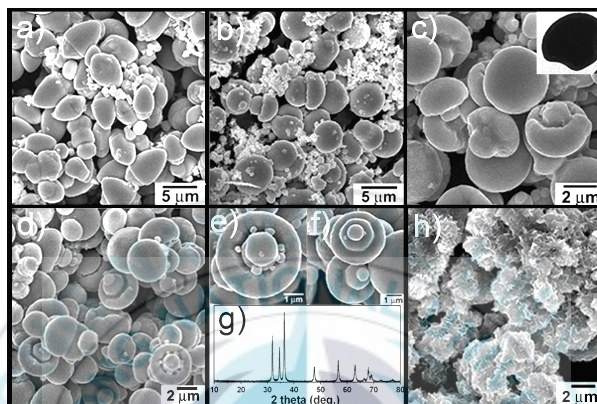


Figure 5-2. FE-SEM images of ZnO samples synthesized with 4.8 mmol $\text{Zn}(\text{NO}_3)_2$, SDBS: Zn^{2+} ratio: a) 1.0, b) 2.0, c) 3.0 and d) 4.0. e) and f) enlarged images of sample in image d). g) XRD pattern of sample in image d). h) FE-SEM image of samples synthesized with 19.2 mmol SDBS, SDBS: Zn^{2+} ratio is 40.

The corresponding XRD of the same products is shown in Figure 5-2g). All peaks can be indexed well with pure wurzite zinc oxide. Compared with XRD in Figure 5-1, the less sharp peaks here also confirm that those mushroom-like structures are aggregated small particles. Furthermore, with constant SDBS amount, decreasing of Zn^{2+} concentration, the mushroom-like morphology of products can be remained. With the SDBS vs. Zn^{2+} ratio is 40, only irregular shape products can be found as presented in Figure 5-2h). The products have the most uniform morphology in Figure 5-2d), thereby the further experimental studies will be carried out with the same concentration of SDBS and Zn^{2+} .

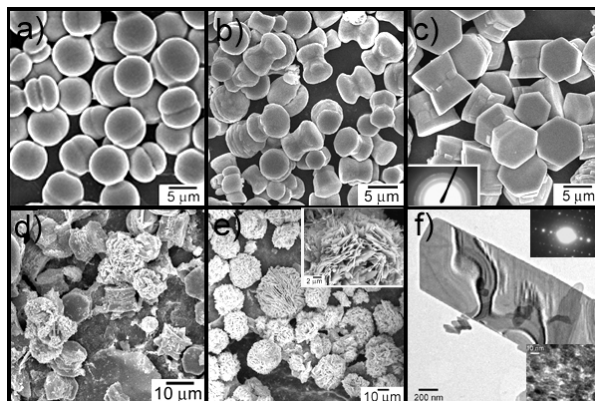


Figure 5-3. FE-SEM images of ZnO samples synthesized with 4.8 mmol $\text{Zn}(\text{NO}_3)_2$ and 19.2 mmol SDBS in ethanol solution: a) 1 mL, b) 2 mL, c) 4 mL, d) 8 mL, e) 24 mL water. c) Inset is corresponding ED pattern of the product. e) Inset is high resolution SEM image of products. f) TEM image of a piece of sheet from sample in e). f) Insets: upside ED pattern, bottom high resolution TEM image from the sheet.

Keeping the SDBS and Zn^{2+} concentration, the influence on products morphology with different amount of water additions is studied subsequently. The anionic surfactant can be made to form micelles with diverse shapes by adjusting experimental parameters. The self-assembled DBS^{2-} layers at the interface of water and ethanol could act as template for growing ZnO. The hydrophilic head of DBS^{2-} can form an anionic surface exposed to water, and thus Zn^{2+} cations can directly attach to the negatively charged DBS^{2-} template to initiate the crystal growth. With water addition introduced into the reaction system, diverse morphological products can be produced by simple adjusting the water volume (Figure 5-3). Firstly, the products with two hemi-parts are obtained. For example, in Figure 5-3a) with 1.0 mL water, the spherical products contain two hemispheres. And 2.0 mL water addition produces dumbbell-like products (Figure 5-3b)). Increasing the water volume to 4.0 mL, the products have uniform and regular shapes with two hexagonal prisms. The corresponding SAED rings in the inset of Figure 5-3c) indicates that the hexagonal prism is multi-crystalline structures. Further increase on water volume,

polydisperse samples with their ununiformity on morphologies are observed. In Figure 5-3d), some particles are multilayer while others remain bilayer of hexagonal prisms. When the water volume increased to 20 mL, flower-like aggregated sheets are obtained. Figure 5-3e) shows the products with 24 mL water addition. And the inset shows a high-resolution FE-SEM image taken from a single flower, which clearly shows the aggregation structure of the flower. High resolution TEM observation is used to study the detail information of the products. The sample for TEM is prepared by sonicating the products in ethanol for several minutes before drip on the grid. In Figure 5-3f), a piece of sheet with 0.75 μm width and 10 μm length is observed. Insets of Figure 5-3f) is corresponding SAED spots (top) and high magnification TEM image (bottom), which suggest the sheet is formed by oriented attachment of approx. 4 nm sized small nanoparticles. The aggregative particulate growth involves self-alignment of nanocrystallites along their common crystallographic orientations. Due to their external surfaces are not smooth and there are no crystal facets that can be observed, it is believed that the formation of these nanosheets in the present case is based on the aggregative growth mechanism. A representative XRD pattern of Figure 5-5 demonstrates that the ZnO nanoparticles are very small size.

Fourier transform IR spectroscopy (FT-IR) and X-ray diffraction (XRD) techniques are conjunct with the above microscopy studies. Figure 5-4 shows FT-IR spectra of pure SDBS and products obtained from the reactions with different amount of water addition. A new absorption at ca. 450 cm^{-1} appears in all spectra of the products that confirms the formation of ZnO. And a sharp peak at 3530 cm^{-1} in Figure 5-4c) and d) is characteristic of non-associating H–O stretching vibration that indicates the existence of free hydroxyls.¹⁵ Also in spectra b) a weak absorption

peak can be observed at the same position. The absorptions centered at 2900 cm^{-1} are assigned to C–H stretching vibrations. Absorptions attributed to S–O vibrations in SDBS (ca. 1189 cm^{-1}) can be detected in products. And absorption at 1130 cm^{-1} shifts to 1120 cm^{-1} . Based on the above discussion, it is concluded that Zn^{2+} cations have strong interactions with the sulfonate radicals of SDBS with increased water addition.

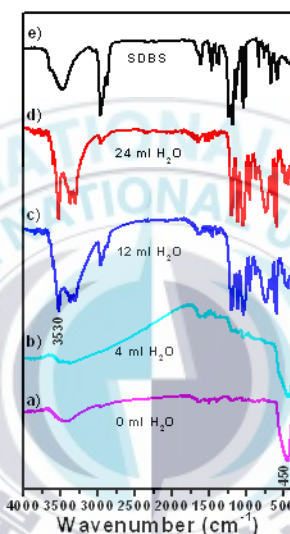


Figure 5-4. FT-IR spectra of pure SDBS and ZnO samples synthesized with 4.8 mmol $\text{Zn}(\text{NO}_3)_2$ and 19.2 mmol SDBS in ethanol solution: 0 mL, 4 mL, 12 mL and 24 mL water.

This interactions phenomenon can be demonstrated by XRD detection. Figure 5-5 shows XRD patterns of the products obtained from the reactions containing different amount of water addition. At the first stage, with small amount of water added into the reaction system, the hydrolysis of $\text{Zn}(\text{NO}_3)_2$ is accelerated, therefore after the same reaction time the product has better crystalline structure as the XRD peaks are becoming sharp with higher intensity (as shown in Figure 5-5). On the other hand, the water addition will also increase the interaction between Zn^{2+} and sulfonate radicals of SDBS, thus with further increase on water addition, the multi-phase

products is obtained. With large amount of water, the small sized ZnO particles are produced as the peaks of ZnO are becoming weak and broad. The XRD result demonstrates the TEM observation that the nanosheets are formed by oriented attachment of small size ZnO nanoparticles.

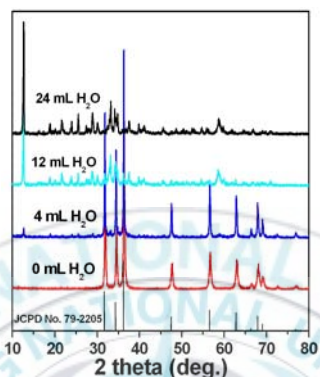


Figure 5-5. XRD patterns of ZnO samples synthesized with 4.8 mmol $\text{Zn}(\text{NO}_3)_2$ and 19.2 mmol SDBS in ethanol solution: 0 mL, 4 mL, 12 mL and 24 mL water.

With NaOH added into the ethanol water solution reaction system, bi-layer hexagonal disks can be obtained as shown in Figure 5-1. As well as we know, the anionic surfactant usually forms self-assembled double layers and multilayers in lamellar micelles. The Zn^{2+} (0001) surface bonds strongly to DBS^{2-} due to charge interaction, and the densely packed DBS^{2-} will protect the surface from further “etching” or reaction, resulting the formation of the flat side of the disks. The DBS^{2-} template stabilizes the surface charge and the structure, therefore the fast growth along $\langle 2\text{-}1\text{-}10 \rangle$ leads the formation of hexagonal disks enclosed by $\{10\text{-}10\}$ facets. The growth of ZnO disks can take place simultaneously on both sides of the template and thus result in back-to-back growth of bi-layer hexagonal disks. Figure 5-6 exhibits the influence of surfactant amount on the bi-layer structures. The ethanol water solution contains 3 mL water, 2.4 mmol zinc nitrate, 3.6 mmol NaOH,

and series increased SDBS from 1.2 mmol to 19.2 mmol. The diameter of the products maintains at approximate 1.7 μm and the thickness decreases from ca. 650 nm to 100 nm along with the increasing of surfactant amount. And the products prepared with 19.2 mmol SDBS shows irregular rough edges. Free surface sites are available for growth once Zn^{2+} ions have reached the surface. Crystal growth is probably not limited by incorporation of Zn^{2+} to the crystal, but rather by the transport to the crystal surface through the thick hydrophobic alkyl chain of SDBS. High concentration of SDBS generates thicker alkyl chains but shorter alkyl chain block, which provides the best shielding of the growth sites on the crystal surface toward the solution via a large amount of swollen hydrophobic alkyl chain coils. This presumably slows down the diffusion of Zn^{2+} to the surface of the growing crystal and allows for a well-defined growth process because the Zn^{2+} delivery to the growth sites is slower than using low concentration of SDBS. The short solution block limits the anchor block-to-anchor block distance on the crystal surface at a short length scale (the closest solution block-solution block distance is dominated by the radius of gyration of the swollen alkyl chain block.) The short solution block reduces the number of undisturbed growth sites available and forces the formation of crystals with various morphologies as observed in Figure 5-6c), e) and g). However, short solution block also limits the Zn^{2+} resources to transport through the thick hydrophobic alkyl chains for crystal growth and produce thin disks.

The morphologies of the products in Figure 5-6a) and c) can be obtained at lower reaction temperature (140 $^{\circ}\text{C}$) by prolonging the reaction time or increasing NaOH amount as shown in Figure 5-7. Small amount of NaOH leads the formation of wafers and large plates (Figure 5-7a)), no bi-layer hexagonal disks can be found. Increasing NaOH amount, bi-layer hexagonal disks and wafers coexist (Figure

5-7b)). Or with prolonged reaction time, the products in Figure 7a) changes to bi-layer hexagonal disks. Products in Figure 5-6a) can grow longer with prolonged the reaction time to 8 h, and the aspect ratio (defined as plate thickness vs. plate diameter) gradually increases from 0.34 to 2.4. Without any surfactant to counterbalance the charge, crystal growth prefers to occur on the (000-1) facet, thus prolonging the reaction time will obtain products with high aspect ratio. The similar phenomenon can be observed in none NaOH addition experiment, as shown in Figure 5-8, with prolonging reaction time to 8 h, the aspect ratio increases from 0.5 to 1.0. The energy dispersive spectroscopy (EDS) is performed around the hexagonal surfaces and the interfaces of individual bi-layer hexagonal structures. As expected, the interface region is bound by the (000-1) plane rich in O^{2-} anions (atomic ratio of Zn/O = 0.846), whereas the hexagonal surfaces were bound by the (0001) plane rich in Zn^{2+} cations (atomic ratio of Zn/O = 0.856). Same result is observed on the products in Figure 5-7d), atomic ratio of Zn/O at the interface region is 0.946, while atomic ratio of Zn/O at the hexagonal surfaces rich is 0.985 (Figure 5-8c)).

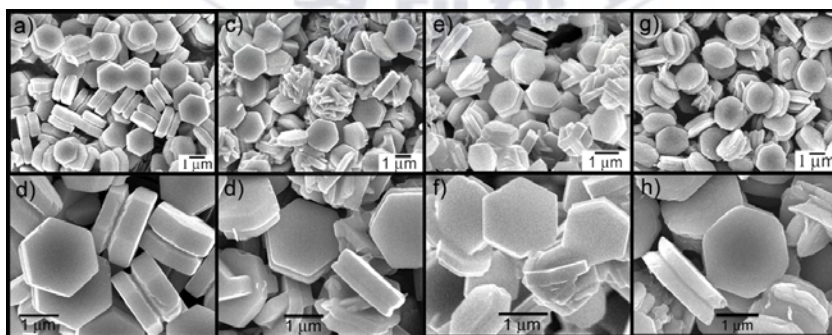


Figure 5-6. FE-SEM images of ZnO samples synthesized with 2.4 mmol $Zn(NO_3)_2$ in ethanol solution with 3 mL water: a) and b) 1.2 mmol, c) and d) 2.4 mmol, e) and f) 4.8 mmol, g) and h) 19.2 mmol SDBS.

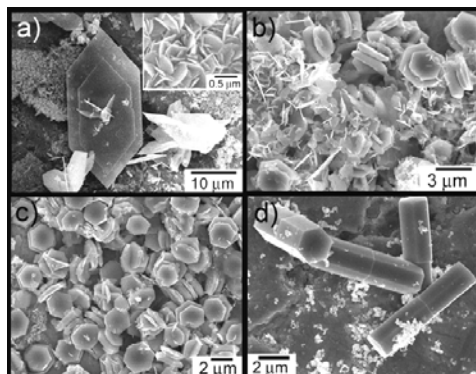


Figure 5-7. FE-SEM images of ZnO samples synthesized in ethanol solution with 3 mL water with different reaction parameters. 1.2 mmol SDBS: a) 2.4 mmol NaOH, 140 °C 4 h; b) 3.0 mmol NaOH, 140 °C 4 h; c) 2.4 mmol NaOH, 140 °C 10 h; d) 3.6 mmol NaOH, 180 °C 8 h.

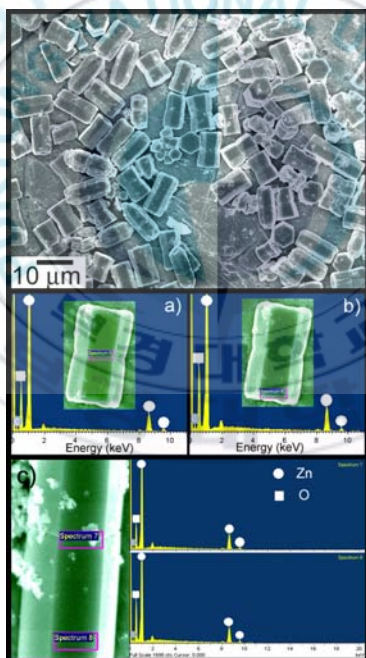


Figure 5-8. FE-SEM image and EDS spectra of ZnO samples synthesized with 4.8 mmol $\text{Zn}(\text{NO}_3)_2$ and 19 mmol SDBS in ethanol solution with 3mL water reacted for 8 h. a) the interface and b) hexagonal surface of an individual bi-layer hexagonal structure. c) EDS spectra of the interface (top) and hexagonal surface (bottom) of ZnO samples in Figure 5-7.d).

5.4. Conclusion

In summary, a novel surfactant-directed solvothermal synthesis approach has been successfully demonstrated on fabricating large scale of ZnO hybrid materials with diverse morphologies in a simple ethanol solution. By adjusting the reaction parameters, the morphology of products can be easily controlled ranging from mushroom-like, double hemispheres, dumbbell, bi-layer hexagonal prisms, to flower-like aggregated sheets and bi-layer hexagonal disks. Due to the charge compensation of the anionic DBS²⁻ template at the Zn²⁺ (0001) surface of ZnO, the fast growth along <2-1-10> forms hexagonal disks enclosed by {10-10} facets. Because of the polar structure of ZnO crystal, bi-layer morphologies are the most common structure. In addition, the synthetic flexibility of the present surfactant-directed ethanol solution approach creates an environmental benign route for morphology controlled synthesis of inorganic hybrid materials on large scale.

References

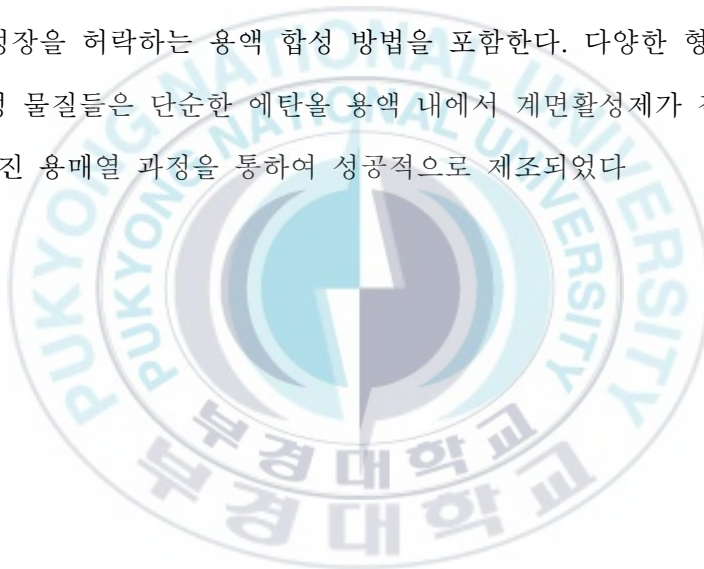
1. (a) Sun, S.; Murray, C. B.; Weller, D.; Folks, L.; Moser, A. *Science* **2000**, 287, 1989; (b) Aizpurua, J.; Hanarp, P.; Sutherland, D. S.; Käll, M.; Bryant, G. W.; García de Abajo, F. J. *Phys. Rev. Lett.* **2003**, 90, 57401; c) Schmid, G. *Nanoparticles: From Theory to Application*, Wiley-VCH, Weinheim, Germany **2004**.
2. (a) Dumestre, F.; Chaudret, B.; Amiens, C.; Renaud, P.; Fejes, P. *Science* **2004**, 303, 821; (b) Li, F.; He, J.; Zhou, W.; Wiley, J. B. *J. Am. Chem. Soc.* **2003**, 125, 16166; (c) Joo, J.; Kwon, S. G.; Yu, J. H.; Hyeon, T. *Adv. Mater.* **2005**, 17, 1873; (d) Qiu, R.; Zhang, X. L.; Qiao, R.; Li, Y.; Kim, Y. I.; Kang, Y. S. *Chem. Mater.* **2007**, 19, 4174; (e) Qiao, R.; Zhang, X. L.; Qiu, R.; Kim, J. C.; Kang, Y. S. *Chem. Mater.* **2007**, 19, 6485.

3. (a) Huang, M. H.; Mao, S.; Feick, H.; Yan, H.; Wu, Y.; Kind, H.; Webber, E.; Russo, R.; Yang, P. *Science* **2001**, 292, 1897; (b) Yang, P.; Yan, H.; Mao, S.; Russo, R.; Johnson, J.; Saykally, R.; Morris, N.; Pham, J.; He, R.; Choi, H.-J. *Adv. Funct. Mater.* **2002**, 12, 323.
4. (a) Saito, N.; Haneda, H.; Sekiguchi, T.; Ohashi, N.; Sakaguchi, I.; Koumoto, K. *Adv. Mater.* **2002**, 14, 418; (b) Park, W. I.; Yi, G.-C.; Kim, J.-W.; Park, S. M. *Appl. Phys. Lett.* **2003**, 82, 4358.
5. (a) Keis, K.; Magnusson, E.; Lindstrom, H.; Lindquist, S. E.; Hagfeldt, A. *Sol. Energy* **2002**, 73, 51; (b) Greene, L. E.; Law, M.; Tan, D. H.; Montano, M.; Goldberger, J.; Somorjai, G.; Yang, P. *Nano Lett.* **2005**, 5, 1231.
6. (a) Liang, S.; Sheng, H.; Liu, Y.; Hio, Z.; Lu, Y.; Shen, H. *J. Cryst. Growth* **2001**, 225, 110; (b) Lee, J. Y.; Choi, Y. S.; Kim, J. H.; Park, M. O.; Im, S. *Thin Solid Films* **2002**, 403, 553.
7. (a) Golego, N.; Studenikin, S. A.; Cocivera, M. *J. Electrochem. Soc.* **2000**, 147, 1592; (b) Lao, J. Y.; Wen, J. G.; Ren, Z. F. *Nano Lett.* **2002**, 2, 1897; (c) Song, J.; Zhou, J.; Wang, Z. L. *Nano Lett.* **2006**, 6, 1656; (d) He, J. H.; Lao, C. S.; Chen, L. J.; Davidovic, D.; Wang, Z. L. *J. Am. Chem. Soc.* **2005**, 127, 16376.
8. Wang, Z. L.; Kong, X. Y.; Zou, J. M. *Phys. Rev. Lett.* **2003**, 91, 185502.
9. (a) Kong, X. Y.; Wang, Z. L. *Science* **2004**, 303, 1348; (b) Kong, X. Y.; Wang, Z. L. *Nano Lett.* **2003**, 3, 1625; (c) Vayssieres, L. *Adv. Mater.* **2003**, 15, 464; (d) Zhang, X. L.; Kang, Y. S. *Inorg. Chem.* **2006**, 45, 4186.
10. (a) Gao, P. X.; Wang, Z. L. *J. Am. Chem. Soc.* **2003**, 125, 11299; (b) Hu J. Q.; Bando, Y.; Zhan, J. H.; Li, Y. B.; Sekiguchi, T. *Appl. Phys. Lett.* **2003**, 83, 4414; (c) Park, W. I.; Yi, G.-C.; Kim, M.; Pennycook, S. J. *Adv. Mater.* **2002**, 14, 1841; (d) Wu, J.-J.; Liu, S.-C. *Adv. Mater.* **2002**, 14, 215.

11. (a) Taubert, A.; Palms, D.; Weiss, Ö.; Piccini, M.-T.; Batchelder, D. N. *Chem. Mater.* **2002**, *14*, 2594; (b) Zhang, J.; Sun, L.; Yin, J.; Su, H.; Liao, C.; Yan, C. *Chem. Mater.* **2002**, *14*, 4172; (c) Yao, K. X.; Zeng, H. C. *J. Phys. Chem. B* **2006**, *110*, 14736; (d) Zhang, X. L.; Qiao, R.; Qiu, R.; Li, Y.; Kang, Y. S. *J. Phys. Chem. A* **2007**, *111*, 4195; (e) Xu, H.; Goedel, W. A. *Angew. Chem. Int. Ed.* **2003**, *42*, 4649.
12. (a) Li, F.; Ding, Y.; Gao, P.; Xin, X.; Wang, Z. L. *Angew. Chem. Int. Ed.* **2004**, *43*, 5238; (b) Peng, Y.; Xu, A.-W.; Deng, B.; Antonietti, M.; Cölfen, H. *J. Phys. Chem. B* **2006**, *110*, 2988; (c) Zhang, J.; Liu, H.; Wang, Z.; Ming, N.; Li, Z.; Biris, A. S. *Adv. Funct. Mater.* **2007**, *17*, 3897.
13. (a) Greene, L. E.; Laq, M.; Goldberger, J.; Kim, F.; Johnson, J. C.; Zhang, Y.; Saykally, R. J.; Yang, P. *Angew. Chem. Int. Ed.* **2003**, *42*, 3031; (b) Hughes, W.; Wang, Z. L. *J. Am. Chem. Soc.* **2004**, *126*, 6703.
14. Joo, J.; Kwon, S. G.; Yu, J. H.; Hyeon, T. *Adv. Mater.* **2005**, *17*, 1873.
15. (a) Pavia, D. L.; Lampman, G. M., Jr. Kriz, G. S. *Introduction to Spectroscopy: A Guide for Students of Organic Chemistry*, Western Washington University; (b) Arenas, J. F.; Marcos, J. I. *Spectrochim. Acta, Part A* **1979**, *35*, 355.

Korean Summary

이 연구에서는 산화아연 그리고 나노와 마이크로 크기의 물질로 이루어진 산화아연의 형상을 제어한 합성방법이 실험적으로 연구되었다. 수직면으로 이루어진 산화아연 나노로드, 1 차원 zinc nickel oxide 고체용액, Ni 와 Co 가 첨가된 ZnO 중공구체가 간단한 용매열 과정에 의하여 성공적으로 제조되었다. 이 합성은 형판과 지지체를 사용하지 않으며, 많은 양을 값싸게 그리고 온건한 온도의 조건하에서 ZnO 나노구조물의 방향성 성장을 허락하는 용액 합성 방법을 포함한다. 다양한 형태를 가진 ZnO 혼성 물질들은 단순한 에탄올 용액 내에서 계면활성제가 직접적으로 사용되어진 용매열 과정을 통하여 성공적으로 제조되었다



Acknowledgements

Special thankfulness is given to professor Young Soo Kang and professor Ju Chang Kim. And I want to thank our department academic staff and our group members for your kindness and help in the last five years.



Publication

1. **Xiao Li Zhang** and Young Soo Kang. "Large-Scale Synthesis of Perpendicular Side-Faceted One-Dimensional ZnO Nanocrystals" *Inorganic Chemistry*, **2006**, 45, 4186;
2. **Xiao Li Zhang**, Young Hwan Kim and Young Soo Kang. "Low-temperature synthesis and shape control of ZnO nanorods" *Current Applied Physics*, **2006**, 6, 796.
3. **Xiao Li Zhang**, Ru Qiao, Ri Qiu, Yan Li, and Young Soo Kang. "Synthesis and Magnetic Properties of One-Dimensional Zinc Nickel Oxide Solid Solution" *J. Phys. Chem. A*, **2007**, 111, 4195.
4. **Xiao Li Zhang**, Young Hwan Kim and Young Soo Kang. "Synthesis and Properties of TiO₂/ZnO Core/Shell Nanomaterials" *Solid State Phenomena*, **2007**, 119, 239.
5. **Xiao Li Zhang**, Ru Qiao, Ri Qiu, Ju Chang Kim and Young Soo Kang. "Fabrication of Hybrid ZnO with Tunable Morphology via Surfactant-Directed Process" (Submitted)
6. **Xiao Li Zhang**, Ru Qiao, Ri Qiu, Ju Chang Kim and Young Soo Kang. "Inorganic Cluster Synthesis and Characterization of Transition Metal-Doped ZnO Hollow Spheres" *Crystal Growth & Design*, **2008** (In press)
7. **Xiao Li Zhang**, and Young Soo Kang. "Fabrication of Monodispersed 1D Zinc Oxide Nanomaterials by a Simple Organic Chemical Solution Route" *Solid State Phenomena*, **2007**, 121, 175.
8. Don Keun Lee, Young Hwan Kim, **Xiao Li Zhang**, Young Soo Kang, "Preparation of Monodisperse Co and Fe nanoparticle using precursor of M²⁺-oleate₂ (M = Co, Fe)" *Current Applied Physics*, **2006**, 6, 786.
9. Ri Qiu, **Xiao Li Zhang**, Ru Qiao, Yan Li, Young Ii Kim and Young Soo Kang, "CuNi Dendritic Material: Synthesis, Mechanism Discussion and Application as Glucose Sensor" *Chem. Mater*, **2007**, 19, 4174.

(Most-Accessed Articles in Chemistry of Materials: Sep, 2006, ACS Publications)

10. *Ru Qiao, Xiao Li Zhang, Ri Qiu, Yan Li, and Young Soo Kang*, “Fabrication of Superparamagnetic Cobalt Nanoparticles-Embedded Block Copolymer” *J. Phys. Chem. C*, **2007**, *111*, 2426.
11. *Yan Li, Xiao Li Zhang, Ri Qiu, Ru Qiao and Young Soo Kang*, “Chemical Synthesis and Silica Encapsulation of NiPt Nanoparticles” *J. Phys. Chem. C*, **2007**, *111*, 10747.
(Most-Accessed Articles in Journal of Physical Chemistry C: Sep, 2006, ACS Publications)
12. *Ru Qiao, Xiao Li Zhang, Ri Qiu and Young Soo Kang*, “Fabrication of Superparamagnetic Cobalt Nanoparticles-Embedded Block Copolymer Microcapsules” *Chem. Mater*, **2007**, *19*, 6485.
13. *Yan Li, Xiao Li Zhang, Young Hwan Kim and Young Soo Kang*, “Synthesis and Characterization of Co Nanoparticles by Solventless Thermal Decomposition” *Solid State Phenomena*, **2007**, *119*, 71.
14. *Shi-Yong Zhao, Ru Qiao, Xiao Li Zhang and Young Soo Kang*, “Preparation and Reversible Phase Transfer of CoFe₂O₄ Nanoparticles” *J. Phys. Chem. C*, **2007**, *111*, 7875.
15. *Yan Li, Xiao Li Zhang, Ri Qiu and Young Soo Kang* “Investigation of Co Nanoparticle Assemblies Induced by Magnetic Field” *Journal of Industrial and Engineering Chemistry*, **2008**, *14*, 22.